The S. cerevisiae m6A-reader Pho92 promotes timely meiotic recombination by controlling key methylated transcripts

Jérémy Scutenaire, Damien Plassard, Mélody Matelot, Tommaso Villa, Julie Zumsteg, Domenico Libri, Bertrand Séraphin

https://doi.org/10.1093/nar/gkac640

NAR Breakthrough Article

The *S. cerevisiae* m^{6}A-reader Pho92 promotes timely meiotic recombination by controlling key methylated transcripts

Jérémy Scutenaire[1,2,3,4], Damien Plassard[1,2,3,4], Mélody Matelot[1,2,3,4], Tommaso Villa[5], Julie Zumsteg[6], Domenico Libri[5] and Bertrand Séraphin[1,2,3,4,*]

[1]Institut de Génétique et de Biologie Moléculaire et Cellulaire (IGBMC), 67400 Illkirch, France, [2]Centre National de Recherche Scientifique (CNRS) UMR 7104, 67400 Illkirch, France, [3]Institut National de Santé et de Recherche Médicale (INSERM) U1258, 67400 Illkirch, France, [4]Université de Strasbourg, 67400 Illkirch, France, [5]Université de Paris Cité, CNRS, Institut Jacques Monod, 75006 Paris, France and [6]Institut de Biologie Moléculaire des Plantes, CNRS, Université de Strasbourg, 67000 Strasbourg, France

Received April 22, 2022; Revised July 05, 2022; Editorial Decision July 06, 2022; Accepted July 20, 2022

ABSTRACT

N^6-Methyladenosine (m^{6}A), one of the most abundant internal modification of eukaryotic mRNAs, participates in the post-transcriptional control of gene expression through recruitment of specific m^{6}A readers. In *Saccharomyces cerevisiae*, the m^{6}A methyltransferase Ime4 is expressed only during meiosis and its deletion impairs this process. To elucidate how m^{6}A control gene expression, we investigated the function of the budding yeast m^{6}A reader Pho92. We show that Pho92 is an early meiotic factor that promotes timely meiotic progression. High-throughput RNA sequencing and mapping of Pho92-binding sites following UV-crosslinking reveal that Pho92 is recruited to specific mRNAs in an m^{6}A-dependent manner during the meiotic prophase, preceding their down-regulation. Strikingly, point mutations altering m^{6}A sites in mRNAs targeted by Pho92 are sufficient to delay their down-regulation and, in one case, to slow down meiotic progression. Altogether, our results indicate that Pho92 facilitate the meiotic progression by accelerating the down-regulation of timely-regulated mRNAs during meiotic recombination.

GRAPHICAL ABSTRACT

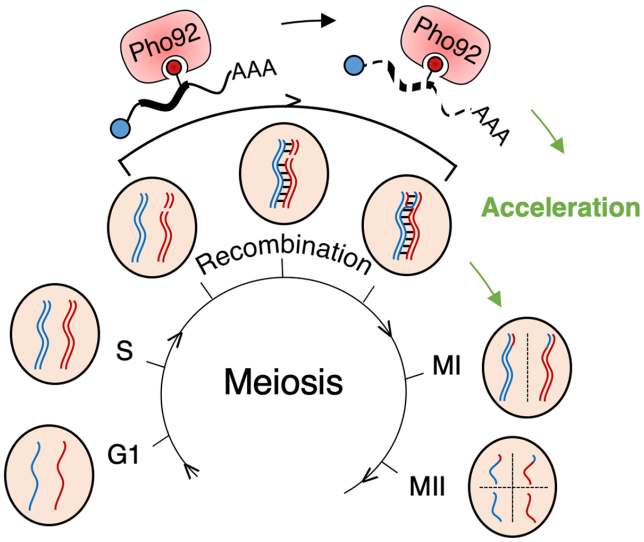

INTRODUCTION

N^6-Adenosine methylation (m^{6}A) is one of the most prevalent internal modification of eukaryotic mRNAs and participates in multiple fundamental processes such as development, cellular differentiation and gametogenesis (1,2). It also emerged as a recent therapeutical target in human neurological diseases and cancer metabolism (3,4). m^{6}A is associated with 2'methyl-ribose as part of the vertebrate mRNA cap structure (5). Moreover, m^{6}A is also found in the body of mRNAs on a subset of RRACH (R: A/G, H: A/C/U)

*To whom correspondence should be addressed. Tel: +33 3 88 65 33 36; Fax: +33 3 88 65 32 01; Email: seraphin@igbmc.fr

sites and enriched in the vicinity of the stop codon in coding sequences and 3′UTR in most organisms (6). On polymerase II transcribed RNAs, m^{6}A is added cotranscriptionally by a multi-component 'writer' complex comprising METTL3-METTL14 heterodimer in metazoans and plants (7,8), of which METTL3 (also called MT-A70) is the active component (9–11). In the yeast *S. cerevisiae*, the METTL3 orthologue is encoded by Ime4 (Inducer of meiosis 4) and associates with 2 non-catalytic factors: Mum2 (Muddled meiosis 2, orthologous to mammalian WTAP), and Slz1 (Sporulation leucine zipper 1) (12,13).

In *S. cerevisiae,* m^{6}A has been detected in transcripts only during meiosis (12–14). Yeast meiosis is part of the sporulation program induced in appropriate conditions in diploid cells that results in the production of 4 haploid spores (15,16). Sporulation is controlled by the transcription factor Ime1 (Inducer of meiosis 1) which activates the 'early' genes, sharing a URS1 (Upstream repression sequence I) site in their promoters, required for DNA replication, programmed formation of DNA double-strand breaks (DSBs) and assembly of synaptonemal complex structures that connect homologous chromosomes during recombination (Figure 1A). *IME1* expression is induced in sporulation conditions but remain repressed by Rme1 (Regulator of meiosis) in haploid cells. A second major meiotic phase involves the transcriptional factor Ndt80 (Non-DiTyrosine) to activate the expression of 'middle genes', containing a MSE (Middle Sporulation Element) motif in their promoters, needed to complete recombination, trigger the two meiotic nuclear divisions (meiosis I and II) and initiate spore formation. In non-meiotic conditions, sporulation genes are transcriptionally repressed by Ume6 (Unscheduled meiotic gene expression 6) and Sum1 (Suppressor of Mar1-1) which bind to URS1 and MSE sites, respectively. Beyond transcriptional control, entry and progression into sporulation requires multiple coordinated regulatory pathways including RNA modifications (14), translational regulation (17), precise post-translational modifications and fine-tuning of protein levels (18).

Meiotic expression of the *IME4* gene encoding the m^{6}A-methyltransferase is tightly regulated ensuring that m^{6}A is only present in diploid cells in sporulation conditions (19,20). Interestingly, variability in the meiotic phenotype of the *ime4Δ/Δ* mutant between various yeast strains was attributed to the presence or absence of a m^{6}A site in the 3′UTR of the *RME1* transcript, that influences its stability (21). Altogether, if the contribution of m^{6}A to yeast meiosis is well established, less progress has been made in understanding how these modifications are decoded and how individual sites could affect sporulation.

m^{6}A has been shown to act in part through m^{6}A readers: RNA-binding proteins specifically recognizing the methylated A. The most-studied readers are YTH domain-containing proteins, represented by one member in yeast, up to five in mammals and over 10 in plants. The mammalian members are divided in two YTHDCs, which were shown to contribute to the regulation of various processes, including nuclear functions such as pre-mRNA alternative splicing and nuclear export (22,23), and three cytoplasmic YTHDFs that accelerate mRNA decay (24,25) and enhance translation efficiency (26,27). More recently, the human YTHDFs were shown to bind equivalently to m^{6}A sites and recruit the CCR4–NOT mRNA deadenylation complex (28). Similar results obtained on orthologues in zebrafish and mouse (29,30) now suggest a unified model in which YTHDFs readers have a conserved role in destabilizing their methylated targets while having limited direct impact on translation. The yeast *S. cerevisiae* encodes a single YTH reader: Pho92 (Phosphate metabolism 92), also known as Mrb1 (Methylated RNA-binding protein 1) (14,31), belonging to the YTHDF group (32). Structural analysis revealed that it recognizes m^{6}A and surrounding residues through a conserved pocket formed by the YTH domain (33). An early study suggested that Pho92 interacts with the CCR4-NOT deadenylation complex to accelerate decay of mRNAs involved in phosphate metabolism (31). However, this function is unlikely imputable to m^{6}A presence as these data have been obtained in haploid cells growing in rich media during which *IME4* expression is repressed and no m^{6}A is detectable (12,19). Thus, although Pho92 is established as a genuine m^{6}A reader, its molecular impact on methylated transcripts remains unexplored.

Here, we show that the m^{6}A reader Pho92 is a meiotic specific factor required for the proper timing of meiotic recombination and subsequent entry into meiotic divisions. By combining high-throughput RNA sequencing and mapping of Pho92-binding sites by UV-crosslinking and analysis of cDNA (CRAC), we show that Pho92 is recruited on specific mRNAs in an m^{6}A-dependent manner and contributes to their down-regulation during the meiotic prophase. Additionally, while functional m^{6}A sites remained ill-defined, we provide evidence that mutating individual m^{6}A sites in key Pho92 targets impairs the temporal control of cognate mRNAs expression and, in one case, delays meiosis. Thus, our analysis reveals the important role of specific mRNA methylation sites in controlling gene expression and cell fate.

MATERIALS AND METHODS

Yeast strains

All yeast strains used in this study are listed in Supplementary Table S5 and were derived from the sporulation-proficient SK1 background either with an endogenous *IME1* promoter or with *CUP1* inducible promoter driving HA-tagged *IME1* expression (*pCUP-IME1*) (34). Gene deletions or tagging-fusions were generated in haploid cells with a one-step PCR replacement protocol using standard lithium acetate transformation protocol (35). Pho92 was C-terminally tagged with TAP (CBP-T7-TEV-ProtA) or HTP (His6-TEV-ProtA) using tagging cassette in pBS2438 and pBS6096 (36), respectively (Supplementary Table S6). Point mutations for *REC8* (A + 1461 > G) and *SAE3* (C + 359 > T and A + 376 > C) were introduced using a 'pop-in/pop-out' strategy (35) using the *URA3* marker and 5-FOA counter selection. The presence of desired mutations was determined by PCR and enzymatic digestion, thanks to a polymorphic restriction site introduced in the mutated version (*REC8* point mutant: new BaeGI site; *SAE3* point mutant: new HaeIII site), followed by sequencing of the PCR products. Diploids were obtained by transformation

of haploid cells with a YCp50 plasmid carrying the *HO* endonuclease gene with *URA3* selection (pBS433). The presence of the *MAT* a and the *MAT* α genes was verified by PCR on isolated colonies. The *HO* containing-plasmid was lost in rich media before further strain use. Plasmids and oligonucleotides used in this study are listed in Supplementary Tables S6 and S7, respectively.

Growth conditions and meiosis induction

Cells in vegetative growth were grown in YPDA (1% yeast extract, 2% peptone, 2% glucose supplemented with 10 mg/l adenine hemisulfate salt) at 30°C and 170 rpm. Synchronous meiotic entry was performed in standard procedure (14). Briefly, respiratory proficient diploids were preselected on 1% yeast extract, 2% peptone, 3% glycerol, 2% agar for 24 h at 30°C, transferred for another 24 h of growth in 1% yeast extract, 2% peptone, 4% dextrose at 30°C and 170 rpm, diluted in BYTA media (1% yeast extract, 2% tryptone, 1% potassium acetate, 50 nM potassium phthalate) to $OD_{600} = 0.2$ and incubated for another 16 h incubation at 30°C and 170 rpm. Next, cells were washed once with sterile milliQ water and resuspended in SPO medium (0.3% potassium acetate) at $OD_{600} = 2.0$ and incubated at 30°C and 170 rpm. For *pCUP-IME1* background, 50 μM of copper (II) Sulfate was added after 2 h in SPO. Cells were isolated from SPO at the indicated time points by centrifugation (3 min at 8000 g).

Western blotting and antibodies

Cells (2 OD_{600} of meiotic cells or of cells grown in YPDA) were collected by centrifugation and stored at −80°C before use. Total proteins were extracted using a published method (37). For Figure 4B, proteins were extracted with an improved version of this method (38). Proteins samples were separated on SDS-PAGE (Tris–HCl gels with 8, 10 or 15% 29:1 acryl:bis-acrylamide) and transferred on Amersham™ Protran™ 0.45 μm nitrocellulose membranes (GE Healthcare, Cat# 10600033) at 4°C for 1 h at 110V. After Ponceau staining, membranes were blocked in 5% milk PBS-T (1× PBS buffer with 0.1% Tween-20) and incubated overnight at 4°C with one of the following antibodies: anti-HA.11 (1:2000; Eurogentec, Cat# MMS-101P-500), anti-Stm1 (1:10 000; kind gift from F. Wyers), anti-Hop1 (39) (1:10 000; kind gift from N. Hollingsworth), anti-Hed1 (40) (1:20 000; kind gift from N. Hollingsworth), anti-Hed1 p-T40 (41) (1:50 000; kind gift from N. Hollingsworth). After four washes in PBS-T, membranes were incubated 1 h at RT with Peroxidase-AffiniPure Goat Anti-Mouse (1:5000; Jackson ImmunoResearch, Cat# 115-035-003) or Anti-rabbit IgG, HRP-linked antibody (1:5000; Cell Signalling, Cat# 7074S). TAP- and HTP-tagged proteins were detected after a unique incubation of the membranes with Peroxidase Anti-Peroxidase Complex produced in rabbit (1:2000; Sigma, Cat# P1291). Chemiluminescence signals were revealed on an Amersham™ Imager 600 (GE Healthcare) apparatus with Immobilon® Crescendo Western HRP Substrate (Millipore, Cat# WBLUR0500) according to the manufacturers' instructions.

Sequences alignment of Pho92 promoter

To align the *PHO92* promoter sequences, the *PHO92* coding and flanking sequences from representative *Saccharomycetaceae* were recovered from the NCBI database using keyword and BLAST searches (42). Sequences upstream of *PHO92*, often extending to the neighboring *WIP1* gene, were aligned using CLUSTAL X (43) and alignments manually edited. Colored alignments were exported from Jalview (44).

Meiotic progression with DAPI counting

Cells (0.3–0.5 OD of 2 OD/ml) were isolated from SPO at the indicated times, centrifuged 3 min at 8000 g, resuspended in 1 volume of 70% ethanol and stored overnight at 4°C. Cells were then pelleted and resuspended in 2 μg/ml DAPI solution in water. Monitoring of meiotic divisions was assayed by counting the number of DAPI masses per cell, in at least 200 cells for each time point, with a Leica DM 4000B microscope equipped with a Hamamatsu ORCA-Flash 4.0 LT C11440 camera.

RNA extraction, northern blotting and RT-qPCR

Total RNAs were extracted on 2.0–3.0 OD of 2 OD/ml yeast cells using a standard hot acid phenol protocol. Frozen cell pellets were resuspended in equal volumes of: 65°C pre-heated 'stabilized phenol water-saturated' pH 4.0 (Eurobio, Cat# GEXPHE01), 50 mM sodium acetate pH 5.5 and acid-washed glass beads (0.5 mm; BioSpec Products, Cat# 11079105) and 1/10e volume of 10% SDS. Samples were then incubated at 65°C for 1 min and vortexed for 30 s, for a total of 3 times, before centrifugation for 10 min (8000 g at 4°C). Recovered supernatants were re-extracted twice with phenol:chloroform:isoamyl alcohol 25:24:1 (Sigma, Cat# 77617) at 4°C and ethanol precipitated.

For northern blot analysis, 5 μg of total RNAs were fractionated by formaldehyde-agarose gel electrophoresis and transferred to Amersham™ Hybond-XL nitrocellulose membrane (GE Healthcare, Cat# RPN203S) by capillarity. After two rounds of UV auto-crosslink (120 000 $\mu J/cm^2$) on UV Stratalinker® 2400 (Stratagene) apparatus, the membranes were probed in hybridization buffer (6× SSC, 2× Denhardt's reagent, 0.1% SDS) at 60°C with primers (Supplementary Table S7) radiolabeled at their 5′-end using T4 Polynucleotide Kinase (NEB, Cat# M0201S) and γ-^{32}P ATP according to the manufacturer's instructions. Radioactive signals were measured using a Typhoon FLA 9000 Phosphorimager (GE Healthcare).

For quantitative RT-PCR, total RNA samples were treated with DNase I recombinant, RNAse-free (Roche, Cat# 4716728001) at 37°C for 1 h and purified by phenol-chloroform extraction as described before. cDNAs were generated from 500 ng of DNase-treated RNAs with SuperScript™ IV reverse transcriptase (Invitrogen™, Cat# 18090050) and oligo(dT)18 primer (Thermo Scientific™, Cat# S0132) according to the manufacturers' instructions. Quantitative PCRs were performed using LightCycler® SYBR Green I Master (Roche, Cat# 04887352001) with primers listed in Supplementary Table

S7 on a LightCycler® LC480 instrument (Roche). Primer efficiencies were >95% and calculated on standard curves generated by a 2-fold dilution series of cDNAs over at least five dilution points measured in triplicate. Each sample was measured in biological triplicates with technical duplicates and transcript abundances were determined using the $2^{-\Delta\Delta Ct}$ method normalized to *ACT1*.

m^{6}A quantification by mass spectrometry

Total RNAs were extracted from yeast meiotic cells as described before and polyadenylated RNAs were isolated from 50 μg total RNAs as starting material with two successive rounds of poly-A selection using Dynabeads™ mRNA Purification kit (Invitrogen™, Cat# 61006) according to the manufacturer's instructions. Absence of rRNA contamination and mRNA integrity were verified with Agilent Bioanalyzer. One hundred nanograms of isolated poly(A)+ RNAs was digested into single nucleosides with 1 U of benzonase® nuclease (Millipore, Cat# E1014-5KU), 0.003 U of Phosphodiesterase I (Sigma, Cat# P3243-1VL) and 1 U of shrimp alkaline phosphatase (NEB, Cat# M0371S) in a 50 μl buffer containing 10 mM Tris–HCl pH 8.0, 1 mM $MgCl_2$ and 0.1 mg/ml BSA. After an incubation for 6 h at 37°C, samples were filtered on Nanosep 3K omega tubes (Pall, Cat# OD003C34) by centrifugation at 12 000 g for 10 min. Ten microliters aliquots were analyzed by LC–MS/MS analysis on an EvoQ Elite TQ (Bruker) equipped with a Dionex UltiMate 3000 UHPLC system (Thermo) coupled to an electrospray ionization source (ESI). Chromatographic separation was achieved using an Acquity UPLC HSS T3 column (100 × 2.1 mm, 1.8 μm; Waters) and precolumn (5 × 2.1 mm, 1.8 μm; Waters). The mobile phase consisted of (A) water and (B) methanol, both containing 0.1 % formic acid. The run started by 0 min of 98% A, then a convex gradient (curve number 5) was applied to reach 7% B at 4 min then another 8-min concave gradient (curve number 8) to reach 100% B and maintained 0.5 min. Return to initial conditions was achieved in 1 min and maintained 1.5 min. The total run time was 15 min. The column was operated at 35°C with a flow-rate of 0.32 ml/min. Nitrogen was used as the drying and nebulizing gas. The nebulizer gas flow was set to 35 l/h, and the desolvation gas flow to 30 l/h. The interface temperature was set to 350°C and the source temperature to 300°C. The capillary voltage was set to 3.5 kV; the ionization was in positive mode. Low mass and high mass resolution were 2 for the first mass analyzer and 2 for the second. The transitions were, in positive mode: adenosine 268.0 > 136.10 and 268.0 > 119.10 (collision energy 15 and 42 V, respectively); N^6-methyladenosine 281.9 > 150.10 and 281.9 > 123.10 (collision energy 17 and 41 V respectively). Data acquisition was performed with the MS Workstation 8 for the mass spectrometry and the liquid chromatography was piloted with Bruker Compass Hystar 4.1 SR1 software and Chromeleon Xpress (Thermo). The data analysis was performed with the Bruker MS Data Review software (version 8.2.1).

Standard solutions of adenosine (0.05, 0.1, 0.5, 1, 5, 10 ng/ml; Sigma, Cat# A9251) and N^6-methyladenosine (0.05, 0.1, 0.5, 1, 5 ng/ml; Selleckchem, Cat# S3190) were used for the quantification. All the calculated values for the different nucleosides in each sample fell within the standard curve range. The ratio of N^6-methyladenosine to adenosine was calculated based on the calibrated concentrations.

Transcriptome analyses

mRNA-seq libraries were generated from 500 ng of total RNA using TruSeq® Stranded mRNA Library Prep kit and TruSeq® RNA Single Indexes kits A and B (Illumina, Cat#20020595) according to manufacturer's instructions. Quantity and quality of the started material and final librairies were checked using a Qubit™ fluorometer (Invitrogen™) and Agilent Bioanalyzer. Resulting libraries were sequenced in 50-length Single-Read on a HiSeq 4000 machine (Illumina).

Reads mapping. Reads were mapped onto the SK1 assembly of the *S. cerevisiae* genome (SK1 MvO V1; SK1_SGD_2018_NCSL00000000) using Tophat 2.0.14 (45) and bowtie version 2–2.1.0 (46). Only uniquely mapped reads have been retained for further analyses. Quantification of gene expression has been performed with HTSeq-0.6.1 (47), using intersection-nonempty mode, and annotations coming from the Saccharomyces Genome Database (SGD). Only non-ambiguously assigned reads have been retained for further analyses.

Clustering. Genes with larger average expression have on average larger observed variances across samples, that is, they vary in expression from sample to sample more than other genes with lower average expression. To avoid these genes to overly influence the variance, variance have been stabilized using the rlog (regularized log) function from DESeq2. Principal Component Analysis is based on their normalized and stabilized gene expression level of all samples.

Statistical analysis. Comparisons of interest have been performed using the R 3.5.1 with *DEseq2* version 1.22.1 (48). More precisely, read counts were normalized from the estimated size factors using the median-of-ratios method (49) and a Wald test was used to estimate the *P*-values. *P*-values were then adjusted for multiple testing with the Benjamini and Hochberg method (50).

Temporal clustering. In order to have a better view of the changes in expression of significant genes between each time, a clustering using the Mfuzz (2.42.0) R package (51) has been realized. Only genes with an adjusted p-value lower than 0.05 in the WT time-series analysis and having a $|\log_2$ FoldChange$| > 2$ (calculated according to the time point having the maximum count relative to the time point having the minimum count) has been retained for clustering. To measure the transcriptomic and temporal impact of Pho92 and Ime4 deletion, the expression value of the corresponding genes in the mutants were plotted according to the clustering established for the WT strain. Heat maps were build using 'heatmapper' online tool (52).

Flow cytometry analysis of meiotic DNA replication

Two hundred microliters of meiotic cells (at 2 OD/ml) were collected at each time point, resuspended in 70% ethanol

and stored overnight at 4°C. Samples were then spun down, resuspended in 200 μl of solution A (50 mM sodium citrate, 0.1 mg/ml RNAse A (Sigma, Cat# R6513), 0.2 mg/ml Proteinase K (Thermo Scientific™, Cat# EO0491)) and incubated 2 h at 50°C. Cells were pelleted again and resuspended in 500 μl of 50 mM sodium citrate containing 2 μM of SYTOX Green (Invitrogen™, Cat# S7020) and transferred to 5 ml FACS tubes (Becton Dickinson, Cat# 352008). After vortexing, samples were analyzed on the LSR II (BD Biosciences) instrument and BD FACS Diva software. Single cells were gated based on forward and side scattering, FITC-A, and FITC-W. Ten thousand events were counted per sample. Data were analyzed using FlowJo 10 software.

Detection of meiotic double strand breaks by Southern blotting

Yeast cells were collected every hour after transfer to SPO (at 2 OD/ml) as above and genomic DNA was extracted on equivalent of 30 OD (time points: 0, 2, 3 h after transfer to SPO) or 15 OD (time points: 4–9 h) according to the method described for medium-resolution mapping of double strand breaks (53). Up to 5 μg of gDNA was digested with 15 U of SalI-HF® enzyme (NEB, Cat# R3138L) for 3 h at 37°C and separated on 0.9% agarose gel for 16 h at 50 V. Next, the gel was incubated 45 min with shaking in 0.2 N NaOH, 0.6 M NaCl and 45 min in 1 M Tris–HCl pH 7.5, 0.6 M NaCl before transfer under neutral conditions on Amersham™ Hybond-XL nitrocellulose membrane (GE Healthcare, Cat# RPN203S). After one round of UV auto-crosslink (120 000 μJ/cm^2) on UV Stratalinker® 2400 (Stratagene) apparatus, the membrane was hybridized with a random-primed ^{32}P-labeled specific probe using Amersham™ Megaprime kit (GE Healthcare, Cat# RPN1607). The probe was obtained from a 1.45 kb PCR product (primers list in Supplementary Table S7) covering a region of the *ARE1* gene.

Luc7-HTP tagging in *S. pombe*

Schizosaccharomyces pombe cells (972 h- background) were grown at 30°C in YES media (1% yeast extract, 3% glucose, 225 mg/l adenine, uracil, leucine and lysine). C-terminal HTP-tagging of the essential U1-snRNP associated protein Luc7 (SPCC16A11.13) was obtained with a one-step PCR replacement method using a pFA6a-HTP-KanMX6 (pBS6122) plasmid template and introduced with a standard lithium acetate transformation protocol (54). Positive transformants were selected on YES + G418 (200 μg/ml) and verified by PCR. Luc7-HTP functional expression was validated by western blot on total protein extracts (55) obtained from 0.5 OD of cells.

Crosslinking and analysis of cDNA (CRAC)

CRAC was performed essentially as described (56) with minor modifications. To facilitate later normalization between samples during dataset analysis, we used an internal 'spike-in' extract of *S. pombe* expressing an RNA-binding protein fused to the HTP tag. The essential protein Luc7 (30.94 ± 19.0 kDA HTP) with a comparable molecular weight to *S. cerevisiae* Pho92 (36.05 ± 19.0 kDA HTP) was chosen in order to collect both proteins in the same fraction during the gel-free protein fractionation step of the CRAC protocol (see below).

Meiosis was induced as previously described in 500 ml of SPO to OD_{600} = 2.0 at 30°C and 5 h following resuspension in SPO (corresponding to 3 h after *IME1* induction), samples were diluted to a final volume of 2 l with SPO media and UV-irradiated at 254 nm for 80 s using the Megatron W5 UV crosslinking unit (UVO3 Ltd). The control samples 'Pho92-HTP No UV' were directly processed without UV-irradiation. The sample used as 'spike-in' from *S. pombe* cells expressing Luc7-HTP was grown independently in 800 ml of 1× EMM media (EMM Broth, Formedium, Cat #PMD0210) supplemented with 2% glucose and 125 mg/l each of adenine (Sigma, Cat #A2786), L-histidine (Sigma, Cat #H8000), uracil (Sigma, Cat #U750), L-lysine (Sigma, Cat #L5501) and L-leucine (Sigma, Cat #L8000). Cells were grown to OD_{600} = 0.5 at 30°C and then diluted to a final volume of 2 l before UV-irradiation (254 nm for 80 s). All samples were harvested by centrifugation, washed in 35 ml cold PBS and resuspended in 2.5 ml/g of cells (or 1.25 ml/g for *S. pombe* cells) of TN150 buffer (50 mM Tris pH 7.8, 150 mM NaCl, 0.1% NP-40 and 5 mM β-mercaptoethanol) supplemented with 0.4 μM AEBSF (Sigma, Cat# A8456), 0.4 μM Benzamidine (Sigma, Cat# B6506 and cOmplete™, EDTA-free Protease Inhibitor Cocktail (Roche, Cat# 11873580001). The suspension was flash frozen in droplets, then mechanically broken through 5 cycles of 3 min at 15 Hz in a Mixer Mill MM 400 (Retsch, Cat# 20.745.0001) and resulting cell powders stored at −80°C until use.

Cell powders were thawed and an amount of *S. pombe* lysate corresponding to 50 OD_{600} (roughly 0.2 g of cells) was added to each *S. cerevisiae* sample, giving a final 5% fraction of *S. pombe* over *S. cerevisiae* cells based on OD_{600}. The resulting lysates were treated for 1 h at 18°C with DNase I (165 U/g of cells) in the presence of 10 mM $MnCl_2$ to solubilize chromatin and then centrifuged at 4800 g for 20 min at 4°C. The supernatant was moved to a fresh tube and further clarified by centrifugation at 22 000 g for 30 min at 4°C. Cleared lysates were incubated with 200 μl Dynabeads™M-280 tosylactivated (Invitrogen™, Cat#14203) coupled with rabbit IgG (15 mg of beads per samples; Sigma, Cat# I5006), nutating at 4°C for 2 h. Beads were washed three times with 10 ml TN1000 (same as TN150+ protease inhibitors, but with 1 M NaCl) for 5 min, and once with 10 ml TN150. His-tagged protein–RNA complexes were eluted from IgG beads with 5 μl homemade recombinant GST-TEV protease for 2 h at 18°C with shaking in 600 μl TN150 supplemented with 0.4 μM oligo (dT), 3 mM $MgCl_2$ and 2 μl (10 U) RNase H (NEB, Cat# M0297S) in order to digest poly(A) tails from RNAs at the same time, thus favoring subsequent reads mapping. Eluate were then treated with 0.1 U RNace-IT RNase cocktail (Agilent, Cat# 400720) for 5 min at 37°C to fragment protein-bound RNA. The RNase reaction was quenched with the addition to 400 mg guanidine hydrochloride. The solution was adjusted for nickel affinity purification to 0.3 M NaCl and 15 mM imidazole, added to 80 μl washed Ni-NTA agarose nickel beads slurry (Qiagen, Cat#

30230), and transferred to Pierce™ Spin Columns – Snap Cap (Thermo Scientific™, Cat# 69725).

Following an overnight incubation at 4°C, nickel beads were washed twice with Wash Buffer I (6.0 M guanidine hydrochloride, 50 mM Tris–HCl pH 7.8, 300 mM NaCl, 0.1% NP-40, 10 mM imidazole and 5 mM β-mercaptoethanol), and then three times with 1× PNK buffer (50 mM Tris–HCl pH 7.8, 10 mM $MgCl_2$, 0.1% NP-40 and 5 mM β-mercaptoethanol). Subsequent reactions were performed on the columns in a total volume of 80 μl, ending each time by one wash with Wash Buffer I and three washes with 1× PNK buffer, in the following order:

1. Phosphatase treatment (1× PNK buffer, 50 U QuickCIP (NEB, Cat# M0525L), 80 U RNaseOUT (Invitrogen, Cat#10777019); 37°C for 30 min).
2. 3′ linker ligation (1× PNK buffer, 800 U T4 RNA ligase 2 truncated KQ (NEB, Cat#M0373L), 80 U RNaseOUT, 1 μM preadenylated 3′ linkers, modified for sequencing from the 3′ end (list in Supplementary Table S7); 25°C (for 5.5 h).
3. 5′ end phosphorylation (1× PNK buffer, 20 U T4 PNK (NEB, Cat# M0201L), 80 U RNaseOUT, 1.5 mM ATP; 37°C for 45 min).
4. 5′ linker ligation (1× PNK buffer, 40 U T4 RNA ligase I (NEB, Cat# M0204L), 80 U RNaseOUT, 1.25 μM 5′ linker (L5 miRCat), 1 mM ATP; 16°C overnight).

The beads were washed three times with Washing Buffer II (50 mM Tris–HCl pH 7.8, 50 mM NaCl, 0.1% NP-40, 10 mM imidazole and 5 mM β-mercaptoethanol). Protein–RNA complexes were eluted for 2 × 10 min in 200 μl elution buffer (same as Washing Buffer II but with 150 mM imidazole). Eluates from control samples (Pho92-HTP No UV × 2 rep + WT × 2 rep) were mixed together as well as eluates from samples (Pho92-HTP × 2 reps + Pho92-HTP *ime4Δ/Δ* × 2 reps) before concentration with Vivacon® 500 filtration cartridges (10 kDa MWCO; Sartorius, Cat# VN01H02) to a final volume of 120 μl. The protein fractionation step was performed with a Gel Elution Liquid Fraction Entrapment Electrophoresis (Gelfree 8100) system (Expedeon, Cat# 48100). Final fractions were treated with 100 μg of proteinase K (Roche) in buffer containing 0.5 % SDS for 2 h at 55°C with shaking. RNA was isolated with phenol:chloroform extraction followed by ethanol precipitation.

RNA was reverse transcribed using SuperScript™ IV reverse transcriptase (Invitrogen™, Cat# 18090050) and the RT L3-2 oligo for 1 h at 50°C in a 20 μll reaction. Samples were heat inactivated (80°C, 10 min) and then treated with 1 μl (5 U) RNase H (37°C, 30 min). The absolute concentration of cDNAs in the reaction was estimated by quantitative PCR using a standard of known concentration. Then, cDNA was amplified by PCR in separate 25 μl reactions each containing 2 μl of cDNA for 11–13 cycles using 0.5 μl (2.5 U) LA Taq (Takara, Cat# RR002M) with P5-3′ and miRCat-PCR-2 oligos at an annealing temperature of 58°C. The PCR reactions were pooled and treated for 1 h at 37°C with 25 U of Exonuclease I (NEB, Cat# M0293S) per 100 μl of pooled PCR reactions. Libraries were purified using NucleoSpin Gel and PCR Clean-up (Macherey-Nagel) and quantified with a Qubit Fluorometer and the Qubit dsDNA HS Assay Kit (Invitrogen, Cat# 740609). Single-end sequencing was performed using Illumina technology on a NextSeq 500 instrument.

CRAC peak calling

CRAC datasets were analyzed as previously described (57) except for the normalization step. Briefly, data preprocessing steps include the 5′ adapter trimming, PCR duplicates and poly-A stretch removal and the reverse complement of the reads. BAM files were generated using bowtie2 (2.4.1) and the *S. cerevisiae* genome (SK1 assembly). The peaks were detected using the extractPeaks pipeline of the PeakCcall suite after gaussian kernel smoothing of the CRAC signal (57) and scored according to the 'h^2w' score, where 'h' = height, and 'w' = width of the peak. The normalization between samples was done according to the internal Luc7-HTP spike-in. For that, the reads that did not map to the *S. cerevisiae* SK1 genome were mapped to the *Schizosaccharomyces pombe* genome (version ASM294v2) after filtering for a minimal length of 40 nt to avoid cross-species mapping. PeakCcall was used to determine the binding score of Luc7-HTP to its U1 snRNA target at the locus (chr II:3020203–3020352) in each sample. The resulted score was used to normalize the score of all *S. cerevisiae* peaks of the respective sample and relative to 'Pho92-HTP Replicate 1' sample. Only the peaks having a score >0.9 were considered as *bona fide* peaks, corresponding to scores above the 98.4 percentiles of the distribution of all peak scores in the 'Pho92-HTP Replicate 1' sample. The intersection of the peaks was made between the two replicates of Pho92-HTP according to the barycentre coordinate of each peak for which –3 and + 3 bases were added, using intersectBed from BEDTools (2.21.0). Annotation of the peaks was carried out using closestBed from BEDTools and the annotation file converted in BED format.

Motif discovery, metagene analysis and gene ontology

De novo motif discovery was performed with the MEME suite (5.4.1) (58) with the default parameters except for the motifs size fixed to nine nucleotides. FASTA sequences corresponding to the different populations of extracted CRAC peaks were used as input.

UTR extensions have been defined according to the file generated in another study (21). The mean length of the 5′UTR, CDS and 3′UTR were calculated and the position of each peak relative to the corresponding mean was determined. To put together the positions of each part of the transcript into a figure, the mean length of the 5′UTR was added to the peak position on the CDS and the mean length of the 5′UTR and the CDS were added to the peak position on the 3′UTR.

Gene ontology was performed either: for Figure 3C, with the GO Term Finder tool from the *Saccharomyces* Genome Database (yeastgenome.org/goTermFinder) using default parameters and a *P*-value threshold of 0.05; or for Figure 5E, with ShinyGO v0.75 (59) using a *P*-value cutoff (FDR) of 0.05.

MazF-qPCR assay for determination of methylation scores

The MazF digestion and qPCR design were based on a described method (60) with few modifications. Briefly, 500 ng of total RNAs, isolated as described before at 3 and 7 h after transfer in SPO, were incubated 2 min at 70°C and placed on ice. Each sample was then incubated at 37°C for 30 min with 20 U of mRNA-Interferase™ MazF enzyme (Takara, Cat# 2415A) in a 10 μl volume reaction containing 1× MazF reaction buffer, 40 U of RNasin® Ribonuclease Inhibitors (Promega, Cat# N2511). All samples were duplicated to include control samples without the MazF enzyme. Reactions were stopped by placing on ice and cDNAs were directly generated from half of each sample using the SuperScript™ IV reverse transcriptase (Invitrogen™, Cat# 18090050) and random hexamer primer (Thermo Scientific™, Cat# SO142). qPCRs were performed as described above using two primers pairs per tested gene. The first 'target' primer pair was designed to flank a putative methylation site with only one ACA site corresponding to the interrogated site, thus amplified only if methylated and not digested by MazF. The second 'control' primer pair was designed to flank an adjacent region in the same gene without an ACA site. The methylation scores of the interrogated site were estimated using the following formula: E (efficiency) $= 2^{-[(Ct\ MazF+)-(Ct\ MazF-)]}$ and methylation scores $= E$ ('target')/E ('control') (60). It relates the transcript abundance of the 'target' amplicon in MazF-treated versus untreated samples, normalized to the transcript abundance of the 'control' amplicon in MazF-treated versus untreated samples.

RESULTS

Pho92: an early meiotic factor

Given the meiosis restricted accumulation of m^6A in budding yeast, we first determined when *PHO92* is expressed. Using a C-terminal TAP-tagged version of Pho92 in the high sporulation efficiency SK1 background, we performed western blot analyses on samples collected during a meiotic time-course. No signal is detected before transfer in sporulation medium (SPO) (Figure 1B, 0 h SPO). Pho92-TAP quickly accumulates after transfer in SPO, peaking after 5–6 h before decreasing. This profile is similar to those observed for *IME4* mRNA and m^6A levels (13) and consistent with changes in the *PHO92* mRNA level (14,61). Strikingly, alignment of the *PHO92* promoter sequences from representative species of the *Saccharomycetaceae* family revealed the presence of conserved motifs including URS1 and MSE (Figure 1C and Supplementary Figure S1A). To test whether these motifs regulate *PHO92* expression through Ime1 and/or Ndt80 during meiosis, Pho92-TAP levels were monitored in *ime1*Δ/Δ and *ndt80*Δ/Δ strains following resuspension in SPO medium. *ndt80*Δ/Δ and wild-type (WT) cells induced Pho92 similarly (Figure 1B), consistent with *NDT80* only being activated around 5 h in SPO (62), indicating that the Pho92 promoter MSE motif is not required for *PHO92* meiotic activation. However, the Pho92-TAP signal persists in the *ndt80*Δ/Δ strain compared to WT, likely as a consequence of the prophase arrest of the mutant, suggesting that Ndt80 activity (indirectly) down-regulates Pho92-TAP at later steps of meiosis. In contrast, no signal was detected during the whole time-course in the *ime1*Δ/Δ mutant (Figure 1B) demonstrating that Ime1 is strictly required for *PHO92* induction, most likely through the highly conserved URS1 element in its promoter.

Given that many meiotic genes are repressed in rich media, we also assessed Pho92-TAP expression during vegetative growth in WT and mutants for Sum1 and Ume6, the factors repressing MSE- and URS1-containing genes, respectively, in non-meiotic conditions. In both WT and *sum1*Δ/Δ cells growing in rich media, Pho92 expression was not detected (Figure 1D). However, deletion of Ume6 allows Pho92-TAP expression in rich media. As no additional protein levels were detected in *sum1*Δ/Δ *ume6*Δ/Δ cells, Ume6 is the main repressor of *PHO92* expression in non-meiotic conditions in diploid and haploid cells (Figure 1D and Supplementary Figure S1B). Accordingly, direct binding of Ume6 to the URS1 element of *PHO92* was recently reported in haploid cells growing in rich media (63) (Supplementary Figure S1C). Altogether, our results indicate that *PHO92* expression is regulated through a conserved URS1 element in its promoter, leading to Ume6-dependent repression in vegetative conditions and early Ime1-dependent activation upon meiosis induction.

Pho92 is required for the proper kinetics of meiosis

Previous studies suggested that *pho92*Δ/Δ mutants have decreased sporulation efficiency or delayed meiosis (14,64). To pinpoint the meiotic function of Pho92, we quantitatively followed the meiotic progression by microscopic observations of DAPI stained cells from *pho92*Δ/Δ and wild-type strains after transfer in SPO medium. To increase meiotic synchronicity, we used a derivative of the SK1 strain (SK1 *pCUP-IME1*) in which the promoter of the meiosis master regulator *IME1* is replaced by the inducible *CUP1* promoter (34). This strain was used for all following experiments unless otherwise stated. In this background, in which *IME1* expression is induced after 2 h in SPO with addition of copper (II) sulfate, meiotic cells (characterized by > 1 nucleus) appear consistently ∼1 h later in the *pho92*Δ/Δ strain compared to WT (Figure 2A). A longer delay ensues from the *ime4*Δ/Δ mutation, consistent with previous observations (14). Detailed analysis indicates that the delay results from defective entry into meiotic nuclear divisions. Indeed, in the absence of Pho92, bi-nucleated cells appear later but the progression between meiosis I and II, assessed by the appearance of tetra-nucleated cells, is not affected (Figure 2B). The overall sporulation efficiency of *pho92*Δ/Δ cells, monitored after 24 h, was similar to WT but was reduced in the *ime4*Δ/Δ mutant (Supplementary Figure S2A). Similar observations were made in the SK1 strain harboring the endogenous *IME1* promoter, even though with lower synchronicity (Supplementary Figure S2B, C), indicating that the *pho92*Δ/Δ defect also arises upon endogenous *IME1* induction. Thus, the Pho92 protein is an early meiotic factor that is required for the proper kinetics of meiosis by regulating early event(s) downstream of *IME1* but prior to, or concomitant with, the first meiotic division.

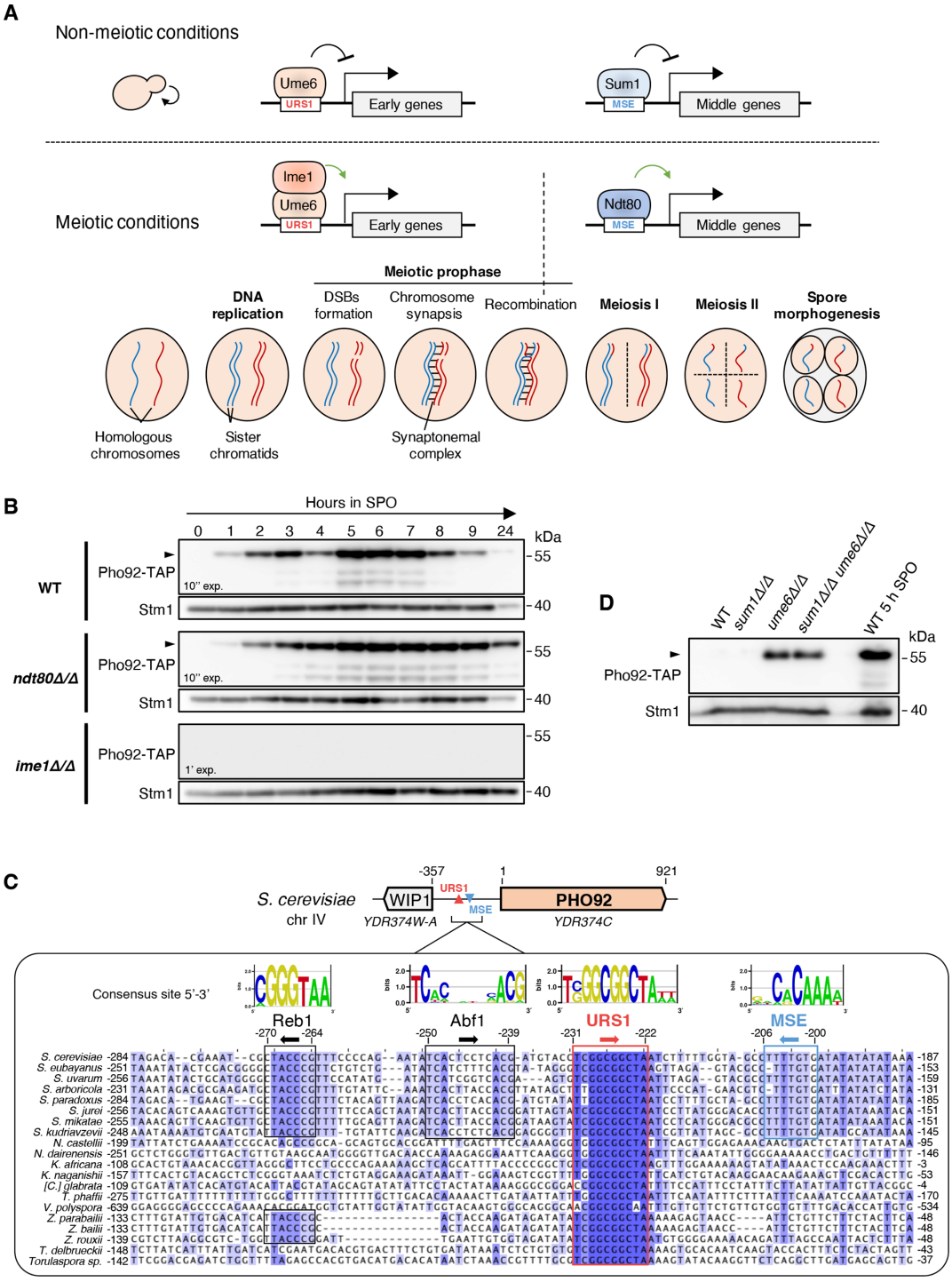

Figure 1. Pho92 is an early meiosis factor transcriptionally regulated in an Ime1/Ume6-dependent manner. (**A**) Schematic model of the transcriptional regulation of early and middle meiotic genes and the different stages of the meiotic program. Early genes are involved in activation of DNA replication and initiation of the meiotic prophase and are regulated by the presence of a URS1 element in their promoters, allowing their repression by Ume6 in non-meiotic conditions and their activation by Ime1 in meiotic conditions. Meiotic middle genes, involved in completion of the meiotic recombination, activation of meiotic divisions and spore formation, contained a MSE motif and are regulated in a Sum1- and Ndt80-dependent manner in non-meiotic and meiotic conditions, respectively. (**B**) Expression of Pho92-TAP during meiosis in diploid strains of the SK1 background. Western blots using Peroxidase Anti-Peroxidase complex to detect Pho92-TAP in total protein extracts from WT, *ndt80Δ/Δ* and *ime1Δ/Δ* cells collected at different hours following resuspension in SPO medium. Stm1 signal detected in the same extracts was used as loading control. (**C**) Sequence alignment of *PHO92* promoters in representative species of the *Saccharomycetaceae* family. The positions indicated are relative to the ATG of *PHO92*. The consensus binding site indicated for each motif or transcription factor is extracted from the YeTFaSCo database (85). (**D**) Expression of Pho92-TAP in diploid strains of the SK1 background grown in rich media. Western blots using Peroxidase Anti-Peroxidase complex to detect Pho92-TAP in total protein extracts from WT, *sum1Δ/Δ*, *ume6Δ/Δ* and *sum1Δ/Δ ume6Δ/Δ* cells collected in log phase cultures grown in rich media (YPDA). Stm1 signal detected in the same extracts was used as loading control.

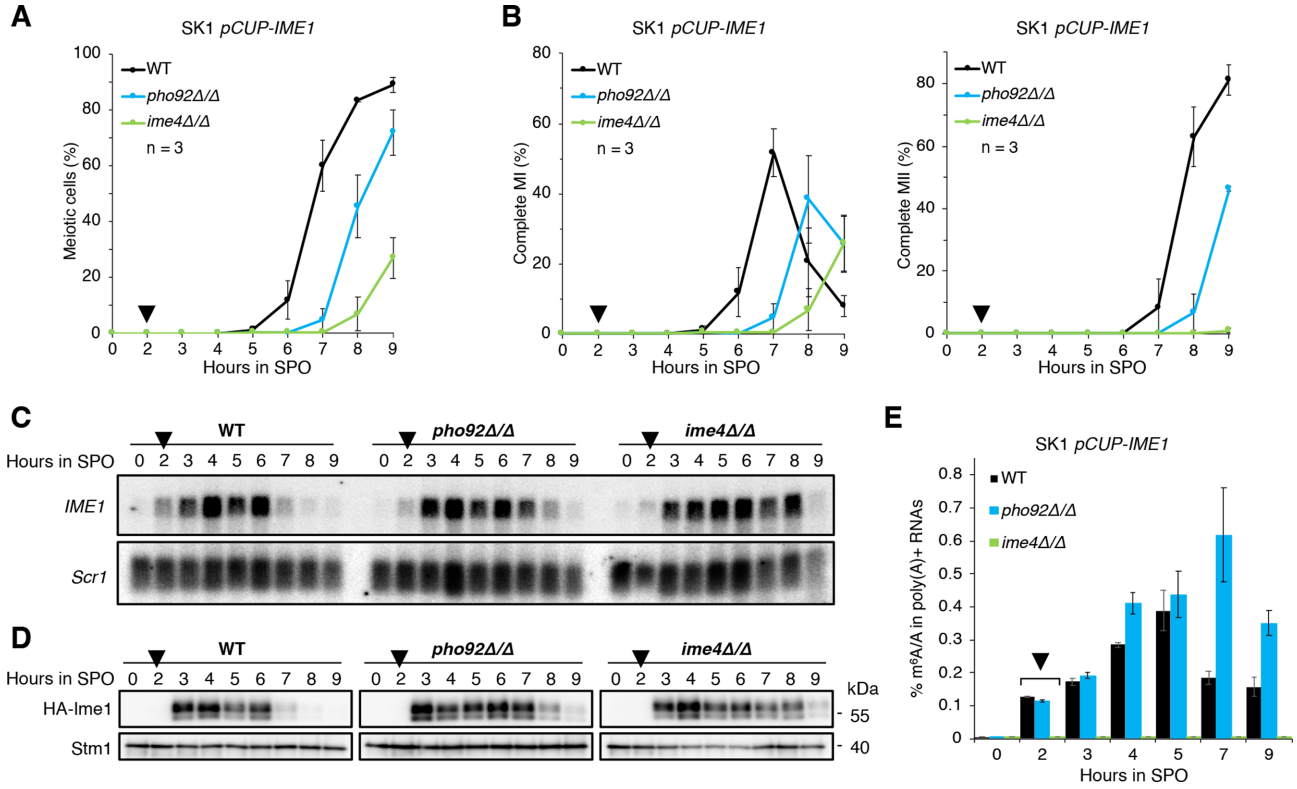

Figure 2. Pho92 is required for the proper timing of meiotic progression and affects *IME1* and m^{6}A down-regulation. (**A**) Kinetics of meiotic cells appearance in WT, *pho92Δ/Δ* and *ime4Δ/Δ* cells following resuspension in SPO medium and induction of *IME1* after 2 h by addition of copper (II) sulfate. Meiotic cells correspond to cells containing >1 nucleus as monitored by DAPI staining on 200 cells per time point. Means and standard deviations from 3 biological replicates. Black triangle above 2 h: time of *IME1* induction. (**B**) Similar to (A) but with the kinetics of cells completing meiosis I (2 nuclei per cell; left panel) and meiosis II (>2 nuclei per cell; right panel). Means and standard deviations from 3 biological replicates. Black triangle above 2 h: time of *IME1* induction. (**C**) Northern blot analysis of *IME1* expression during meiosis in WT, *pho92Δ/Δ* and *ime4Δ/Δ* cells. The ncRNA ScR1 was used as loading control. Black triangle above 2 h: time of *IME1* induction. (**D**) Western blot using anti-HA antibody to detect HA-Ime1 in total protein extracts from WT, *pho92Δ/Δ* and *ime4Δ/Δ* cells collected at different hours following resuspension in SPO medium. Stm1 signal detected in the same extracts was used as loading control. Black triangle above 2 h: time of *IME1* induction. (**E**) LC–MS/MS quantification of m^{6}A relative to A in polyadenylated RNAs extracted during a meiotic time course in two biological replicates of WT, *pho92Δ/Δ* and *ime4Δ/Δ* cells. No m^{6}A was detected at 0-hr SPO nor at any time point of the *ime4Δ/Δ* mutant. Means, minimum and maximum measurements from 2 biological replicates. Black triangle above 2 h: time of *IME1* induction.

Pho92 affects *IME1* and m^{6}A down-regulations at late prophase

We tested whether delayed meiosis resulting from *PHO92* deletion was due to defective *IME1* expression in the *pCUP-IME1* strains. Northern and western blot analyses revealed that *IME1* is strongly induced at mRNA and protein levels in the WT, *pho92*Δ/Δ and *ime4*Δ/Δ strains at 3 h in SPO medium, corresponding to 1 hr after addition of copper (II) sulfate (Figure 2C, D). No *IME1* mRNA nor protein were detected without addition of copper at this time in WT cells (Supplementary Figure S2D). Although the three strains show similar *IME1* induction, its mRNA and protein levels decrease after 6 h in SPO medium in the WT, while they decrease after 7 h in the *pho92*Δ/Δ mutant and after 8 h in *ime4*Δ/Δ cells (Figure 2C, D). Hence, the timing of *IME1* down-regulation correlates with completion of meiosis I which differs for each strain (Figure 2A). Importantly, Rme1, the repressor of *IME1* suggested to be the main target of m^{6}A regulation (21), has no impact on meiotic activation in the *pCUP-IME1* background. Indeed, both the accumulation of the Ime1 protein and meiotic progression are similar in *rme1*Δ/Δ cells compared to WT (Supplementary Figure S2E, F) indicating that m^{6}A acts by other target sites. Overall, these results show that Pho92 does not promote *IME1* activation but rather influences the pathway leading to its down-regulation at middle/late steps of meiosis.

We next monitored the effect of Pho92 on m^{6}A accumulation during meiosis in the *pCUP-IME1* background. The m^{6}A/A ratio present in bulk poly(A) RNAs was quantified by Ultra-Performance Liquid Chromatography-tandem Mass spectrometer. No m^{6}A was detected in the entire time-course in the *ime4*Δ/Δ mutant used as negative control (Figure 2E). In WT cells, m^{6}A appears after 2 h in SPO medium, peaks at the onset of prophase I at 5 h, and decreases afterwards, in agreement with published data (13,14). In the *pho92*Δ/Δ mutant, m^{6}A is similarly induced at 2 hr in SPO but the accumulation continues, reaching a maximum at 7 h, and only starts to diminish afterwards (Figure 2E). This suggests that methylated mRNAs are stabilized or more abundantly produced in the *pho92*Δ/Δ mutant at middle stages of meiosis. Thus, our data reveal that

Pho92 likely influences the duration of meiotic prophase by limiting the persistence of methylated transcripts.

Pho92 affects the meiotic transcriptome during prophase

To unravel the global impact of Pho92 and Ime4 on gene expression during meiosis, we performed poly(A)+ RNAs sequencing on samples collected at different time points (0, 2, 3, 5, 6, 7 and 9 h) following SPO resuspension in biological triplicates of WT, *pho92*Δ/Δ and *ime4*Δ/Δ cells in *pCUP-IME1* background (Figure 3A and Supplementary Figure S3A). We acquired a mean of >22 million reads per sample and obtained normalized expression values (read count ⩾ 1 in at least one sample) on 6092 genes (Supplementary Table S1), covering over 92% of the latest version of the yeast transcriptome (6611 ORFs as of March 2022). Principal component analysis indicates that the three strains have highly related transcriptome profiles at the early time points (up to 3 h) but start to strongly diverge from each other after 5 h in SPO (Figure 3B). Yet, differences are only transient as all strains follow similar trajectories with roughly a 1 h delay for *pho92*Δ/Δ and a 2–3 h delay for *ime4*Δ/Δ. Accordingly, the number of differentially expressed genes compared to WT (fold change ⩾ 2, adjusted *P*-value < 0.05) increases over time after 5 h in SPO medium in both *pho92*Δ/Δ and *ime4*Δ/Δ cells (Supplementary Figure S3B). In line with the more severe phenotype observed in *ime4Δ/Δ*, the number of differentially expressed genes at time points beyond 5 h is between 1.4- and 2.4-fold more important in this strain compared to *pho92*Δ/Δ.

To compare the temporal gene expression profiles between strains, we selected the 4206 genes with an absolute fold change ⩾4 of expression values over the meiotic timecourse in the WT (Figure 3A) and performed a clustering analysis creating 27 clusters of expression profiles (Figure 3C and Supplementary Table S2). Plotting the expression data of these clusters in the *pho92*Δ/Δ and *ime4*Δ/Δ mutants reveals similar waves of expression from 0 to 5 h. Indeed, transcripts of clusters #1–5 and #24–27, enriched in general metabolism and ribosome biogenesis-related biological processes, respectively, are quickly down-regulated following transfer in SPO medium in all strains.

Then, at 3 h in SPO, mRNAs from clusters #10–12, the first with enriched genes involved in meiotic functions, start to accumulate in all strains. While the expression of genes belonging to clusters #10 and #11, enriched in DNA replication and repair functions, is quickly down-regulated at 5 h SPO in all strains, the mRNA belonging to clusters #12 persist longer. Interestingly, these genes, enriched specifically in homologous meiotic recombination and synaptonemal complexes structures, are strongly down-regulated at 6 h in SPO in the WT but remain abundant at this stage in *pho92*Δ/Δ and *ime4*Δ/Δ cells (Figure 3C, detailed in the lower panel), spreading their peak of expression. At 6 h, clusters #14–18, enriched in factors involved in meiotic nuclear divisions and spore morphogenesis, are expressed in the WT strain but their induction is delayed and less prominent in the *pho92*Δ/Δ mutant and even more in the *ime4*Δ/Δ strain. Thus, the transcriptomic analysis reinforces our cellular and molecular analyses indicating that Pho92 and Ime4 have a limited effect on the early meiotic transcriptome but rather affect processes at the onset of meiotic prophase. Interestingly, one of the first clusters affected by inactivation of *PHO92* and *IME4* contains transcripts encoding factors involved in meiotic recombination and synaptonemal complex structures (Figure 3C, lower panel and Supplementary Table S2).

Pho92 temporally influences the formation of meiotic DSBs

To better characterize the impact of Pho92 and Ime4 on meiotic prophase, we first assessed whether they affect DNA replication. Our transcriptomic data indicate that the key genes involved in DNA replication are similarly induced at mRNA levels at 3 h in SPO in WT, *pho92Δ/Δ* and *ime4Δ/Δ* mutants (Supplementary Figure S4A). Consistently, flow-cytometry analysis showed that DNA replicates in similar manner in all strains between 3 and 4 h after resuspension in SPO, corresponding to 1 and 2 h following *IME1* activation (Figure 4A). In contrast, most genes involved in meiotic recombination (belonging to cluster #12, Figure 3C) show an extended expression in *pho92*Δ/Δ and *ime4*Δ/Δ mutants compared to WT (Supplementary Figure S4B). To assess the timing of meiotic recombination, we monitored the phosphorylation of Hop1, an indirect marker of meiotic DSBs formation (65,66), and of Hed1 at Tyr40, a target site of the Mek1 kinase active during the meiotic recombination checkpoint (41,67). Western blots show that both are mostly phosphorylated at 5 h in SPO in the WT (Figure 4B). In contrast, in *pho92*Δ/Δ and *ime4*Δ/Δ mutants, the phosphorylated forms peak at 6 h and p-Hed1 remain detectable for few additional hours in the *ime4*Δ/Δ cells. These observations suggest a delay in meiotic DSBs formation as well as a slightly prolonged DSBs repair in the absence of Pho92, an effect that is even more pronounced in the absence of Ime4. To test this hypothesis, we directly determined the appearance of DSBs by Southern blot at a described hot-spot near the *ARE1* gene (68,69) (Figure 4C, D). In this region, meiotic DSBs are detected at 4 and 5 h in the WT and then disappear afterwards following DSBs repair (Figure 4D). Meiotic DSBs appear 1 h later in *pho92*Δ/Δ and *ime4*Δ/Δ cells and remain visible for few additional hours. While the difference at late meiotic stages between *pho92*Δ/Δ and *ime4*Δ/Δ mutants is clear, regarding the kinetics of meiotic divisions and transcriptome profiles, the initial delay observed in DSBs formation is similar, suggesting that both factors have a comparable effect on meiotic progression until this stage. Thus, our results show that Pho92 and m^6A presence are required for the proper timing of meiotic DSBs formation and in their absence, the meiotic recombination checkpoint, supported by Mek1 activity during DSBs repair, is affected.

Pho92 directly binds methylated mRNAs involved in meiotic recombination

To identify m^6A-dependent mRNA targets bound by Pho92 during meiotic recombination, we performed an improved version of the UV-Crosslinking and analysis of cDNAs (CRAC) technique (36,57) on samples harvested at 5 h in SPO medium. For this procedure, we used cells in *pCUP-IME1* background expressing HTP (His_6-TEV-ProteinA)-tagged Pho92 in WT and in *ime4*Δ/Δ strain to assess for

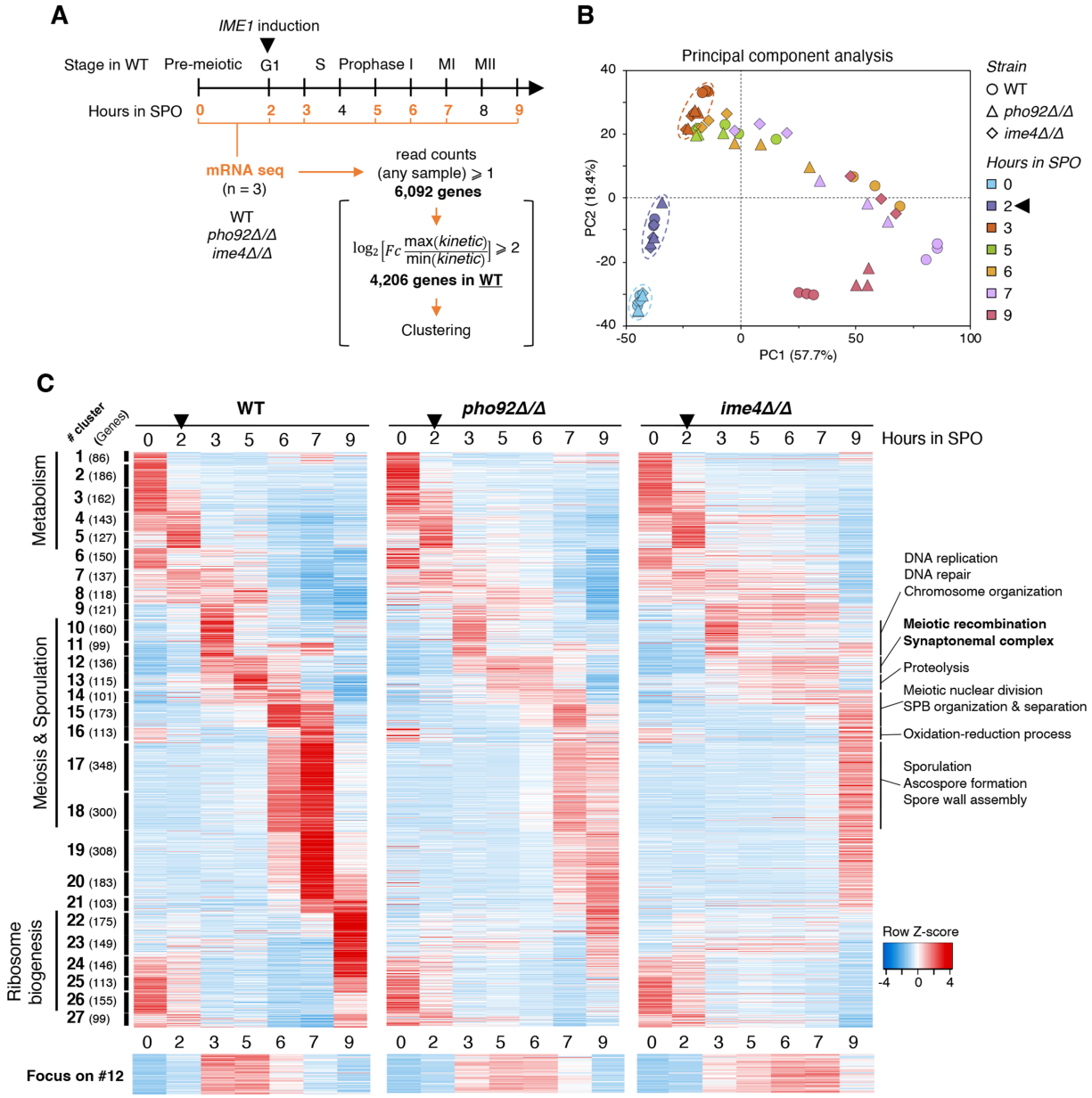

Figure 3. The meiotic transcriptome program is delayed in absence of Pho92. (**A**) Representation of collected samples for mRNA-seq during the meiotic course. The stage in WT cells is indicated above the time line. Time points in orange represent the ones used for mRNA-seq analyses. Below are the criteria used for the genes considered for further analyses and clustering data represented in (C). (**B**) Principal component analysis based on the normalized and stabilized gene expression levels of all samples in three biological replicates. The genotype of the strain is illustrated by the shape of the dot and colors represent the different time points across the meiotic time course. Black triangle at 2 h: time of *IME1* induction. (**C**) Heat map representation of the 4206 genes selected according to criteria in (A) following meiosis induction in WT cells, *pho92Δ/Δ* and *ime4Δ/Δ* mutants. Z-score transformation was performed for each gene considering the mean normalized read count of three biological replicates and scaled from maximum (red) to minimum (blue) expression value from all samples. Genes with similar expression pattern were clustered and arranged together according to the chronology of their respective maximum expression in the WT strain. At the left is indicated the major biological processes enriched in different group of clusters, the number ID of each cluster (#) and, in parenthesis, the number of genes in each cluster. No known biological processes were significantly enriched in clusters #6 to #9 and #19 to #21. At the right, a more detailed list of biological processes is indicated for key meiotic clusters only. Lower panel represents a focus on cluster 12 enriched in genes involved in meiotic recombination and synaptonemal complexes structures. Black triangle above 2 h: time of *IME1* induction.

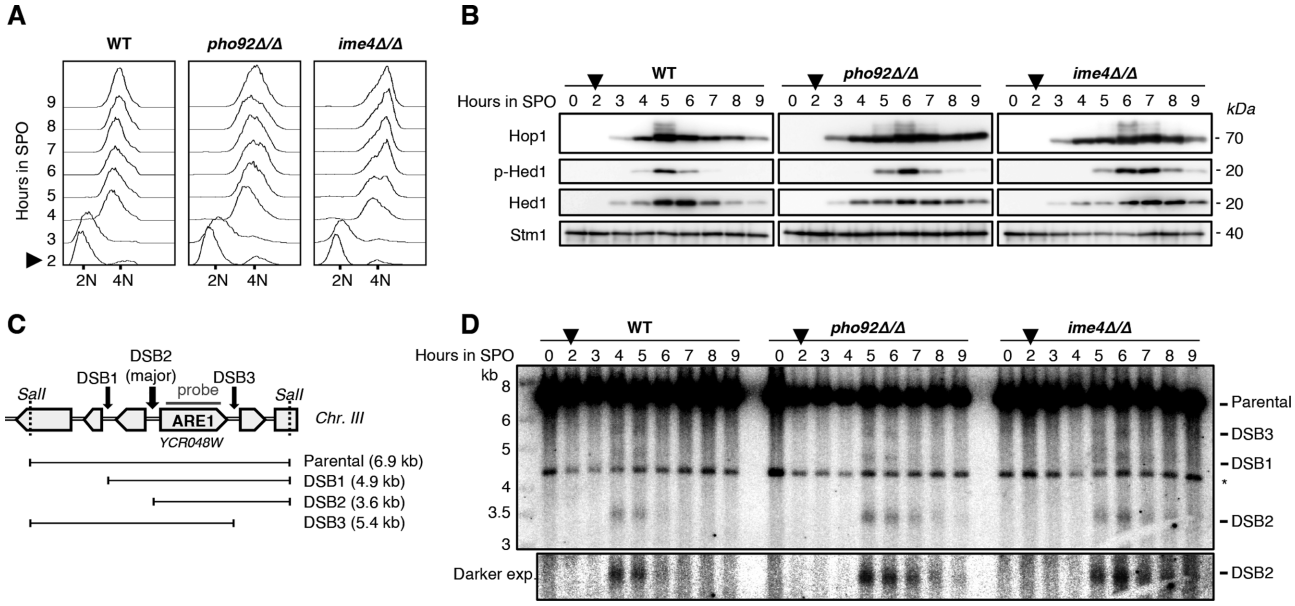

Figure 4. The absence of Pho92 delays meiosis after DNA replication but prior to DSBs formation. (**A**) Flow cytometry analysis of DNA content in WT, *pho92Δ/Δ* and *ime4Δ/Δ* cells across a meiotic time course. Data were collected from cells harvested from 2 h (time of *IME1* induction indicated by a black triangle) to 9 h after resuspension in SPO. At least 10 000 single cells were counted for each time point. Black triangle at 2 h: time of *IME1* induction. (**B**) Western blot analysis of Hop1, p-Hed1 (Hed1 phospho-Tyrosine 40) and Hed1 in total protein extracts from WT, *pho92Δ/Δ* and *ime4Δ/Δ* cells following resuspension in SPO medium. Stm1 signal detected in the same extracts was used as loading control. Black triangle above 2 h: time of *IME1* induction. (**C**) Schematic representation of the *ARE1* region from the chromosome III and the different fragments generated after meiotic DSBs formation and *SalI* enzymatic digestion. The position of the probe used to detect all fragments is indicated in dark grey solid line. (**D**) Southern blot analysis of meiotic DSBs formation in the *ARE1* region in WT, *pho92Δ/Δ* and *ime4Δ/Δ* cells following resuspension SPO medium. An unspecific fragment (*) of ∼4.3 kb is detected from cross reaction of the radiolabeled probe with a *SalI*-generated fragment of the *ARE2* gene, paralogous to *ARE1*. Lower panel represents a focus with darker exposure on the fragment generated by the DSB2, as illustrated in (C). Black triangle above 2 h: time of *IME1* induction.

specific binding to m^{6}A-modified RNAs. Pho92-HTP cells without UV-crosslinking and a wild-type extract, in which no HTP-tagged protein is present, were also used as controls. The functionality of the Pho92-HTP protein was confirmed as the meiosis progression is not delayed in cognate cells and Pho92-HTP protein accumulates with the same profile as the Pho92-TAP version following *IME1* induction, in both the WT and *ime4*Δ/Δ backgrounds (Supplementary Figure S5A, B). Following the CRAC procedure, binding sites were identified in reads presenting a specific deletion induced at UV-crosslinked sites during reverse-transcription and data were normalized using a spike-in of UV-crosslink cells of *Schizosaccharomyces pombe* expressing the essential RNA-binding protein Luc7-HTP (Supplementary Figure S5C and D). The highest numbers of peaks (score > 0.9) were found in the two biological replicates of Pho92-HTP, as expected, with 1061 and 1101 peaks respectively (Supplementary Figure S5E and Supplementary Table S3).

Considering the 794 peaks commonly found in the Pho92-HTP replicates, we classified them according to their scores in the other conditions. We found 627 Ime4-dependent peaks that we further divided in two groups: the 295 peaks with high scores (>4; corresponding to scores above the 99.2 percentile of the distribution of all peaks) in both replicates of Pho92-HTP and at least 2-fold higher than in the *ime4*Δ/Δ mutant (Supplementary Figure S5F), were selected as 'high-score' Ime4-dependent binding sites of Pho92 while the 332 remaining peaks (score < 4 in one replicate of Pho2-HTP) were considered as 'lower-score' (Figure 5A, Supplementary Table S4). In the other control samples, no peaks or peaks with very low score were observed at these sites. The remaining peaks were defined as 'Ime4-independent' binding sites (142 peaks) with scores >2 in *ime4Δ/Δ* mutant, and 'unspecific' sites (25 peaks) with scores >2 in no UV control and/or WT cells (Figure 5A). The 'high-' and 'lower-score' Pho92-binding sites show similar profiles with 259 peaks (87.7%) and 293 peaks (88.2%), respectively, localizing in CDS and predicted UTR regions of 208 and 253 mRNAs (Figure 5B). The majority of the mRNA targets harbor one Pho92-binding site but some have up to seven sites (Supplementary Figure S5G). In contrast, most, if not all, peaks of the 'Ime4-independent' and 'unspecific' groups are found in tRNAs and rRNAs (Figure 5B), thus likely reflecting false positive signals. Strikingly, a single RNA motif of consensus AWRGACDWU was significantly enriched in Pho92-binding sites. It was found in 286 (96,9%) and 324 (97,6%) peaks of the 'high-score' and 'lower-score' binding sites respectively, and matches to an extended version of the established m^{6}A methylation consensus site (Figure 5C and Supplementary Figure S5H). Notably, the position +4 following the central A is strongly biased toward an 'U' residue, found in 97% and 93% of the cases in 'high-score' and 'lower-score' binding sites, respectively. Sequence analysis under the peaks of the other populations did not reveal similar motifs (Supplementary Fig-

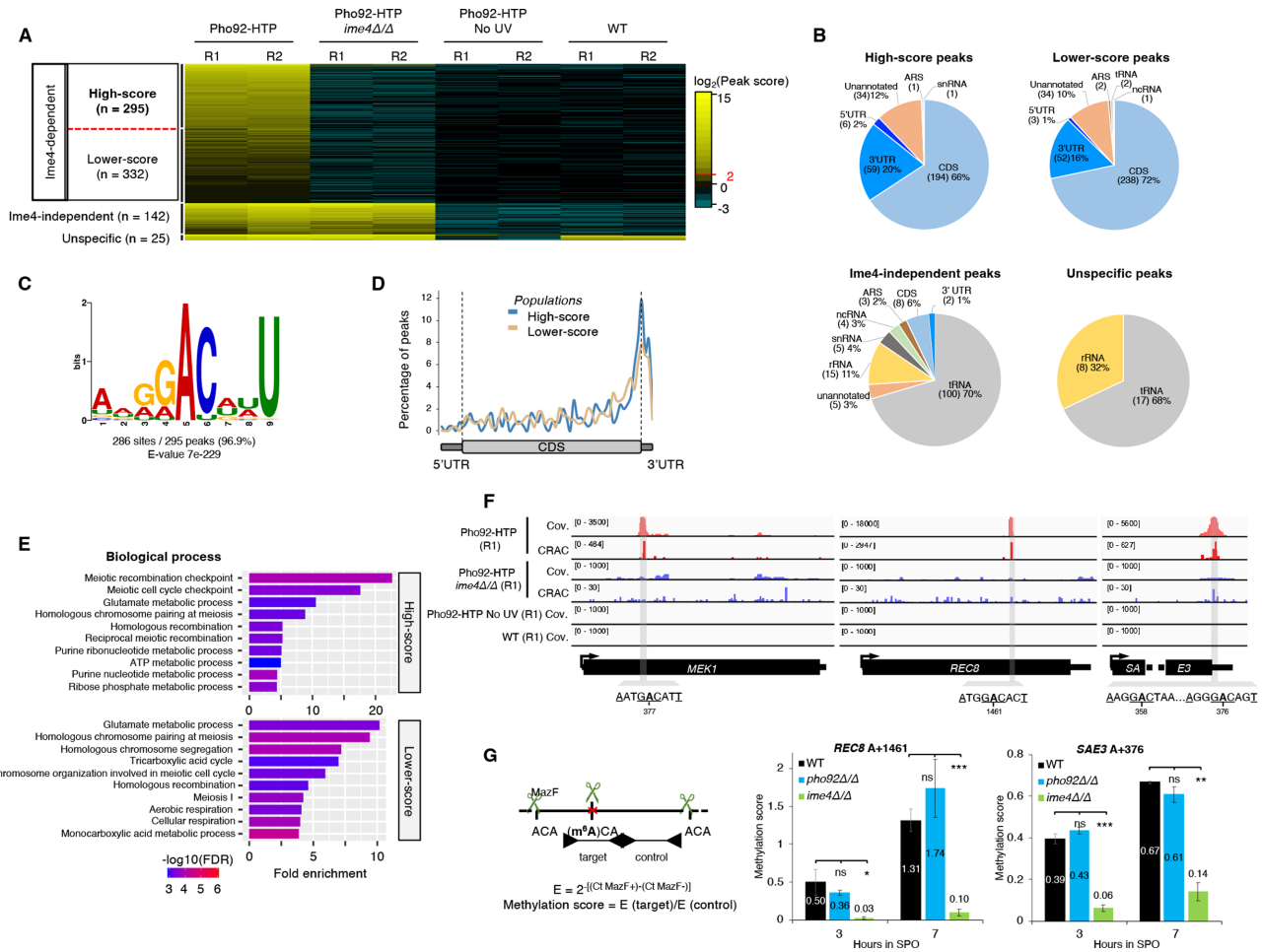

Figure 5. The mRNA targets of Pho92 are mostly bound in an Ime4-dependent manner. (**A**) Heat map representation of the $\log_2$-transformed peak scores for the 794 peaks commonly found in the two biological replicates of Pho92-HTP (scores > 0.9) in the CRAC datasets and their respective values in other conditions (*ime4Δ/Δ* mutant, no UV, WT). Peaks were arranged together according to the fold change score (Pho92-HTP/Pho92-HTP in *ime4Δ/Δ*). (**B**) Pie charts showing peaks distributions in different types of RNA and mRNA regions in the different defined populations. ARS: Autonomous Replication Sequence. (**C**) Sequence motif of the consensus Pho92-binding site as determined by MEME, based on the sequences under the 295 high-score Ime4-dependent peaks. (**D**) Metagene analysis of the Pho92-binding sites based on the peaks' summit positions of the high-score (blue line) and lower-score (light brown line) Ime4-dependent populations. (**E**) Gene ontology enrichment analysis for Pho92-bound transcripts of the high-score (upper panel) and lower-score (lower panel) Ime4-dependent peak populations. Only the top 10 biological processes are shown and ranked according to the fold-enrichment against the genomic background. The $-\log_{10}$ (False Discovery Rate) value of each category is calculated based on nominal *P*-value from the hypergeometric test and indicated in a color scale from maximum (red) to lowest (blue) values. (**F**) IGV tracks showing specific Ime4-dependent binding of Pho92-HTP on *MEK1* (left), *REC8* (middle) and *SAE3* (right) transcripts. Shown are the sequence coverage (Cov.) for each sample and the crosslink signal (CRAC) detected at the UV-crosslinked binding sites. Only values from one biological replicate of each condition are shown. Pho92-binding peaks are highlighted in grey with consensus binding sequences indicated at the bottom and the position of the central 'A' relative to the genomic ATG of each gene. (**G**) Determination of methylation scores of two positions in *REC8* (middle) and *SAE3* (right) transcripts by MazF-qPCR. Samples were taken at 3 and 7 h after SPO resuspension, in which *IME1* was induced after 2 h. Means and standard deviations from three biological replicates. ns: $P > 0.05$, $*P < 0.05$, $**P < 0.01$, $***P < 0.001$, two-tailed *t*-test compared to WT at the respective time point. Left panel: schematic representation of the MazF-qPCR assay and determination of the methylation scores.

ure S5H). Considering only the peaks identified in mRNAs, binding of Pho92 shows a bias toward the 3′ end of coding sequences surrounding the stop codon (Figure 5D). These findings are fully consistent with previous analyses of m^6A sites signature arguing that Pho92 binds methylated mRNAs. However, 98 targets (47%) and 121 targets (47.8%) of the 'high-score' and 'lower-score' populations, respectively, were not identified as methylated candidates in the previous m^6A-seq (14) or MAZTER-Seq (group confidence > 1) (60) analyses (Supplementary Figure S5I). Thus, our approach, that directly target Ime4-dependent binding sites of Pho92, reveals the existence of new potential populations of methylated mRNAs during yeast meiosis.

Gene ontology (GO) analysis revealed that the Pho92 targets are highly enriched in meiotic recombination functions, chromosome pairing, meiosis I and also diverse metabolic processes (Figure 5E). Interestingly, the former group correlates with cluster #12 delayed in *pho92Δ/Δ* cells (Figure 3C) and comprises key meiotic actors involved in checkpoint or components of the cohesin and synaptonemal complexes and the meiotic recombinase (examples in Figure 5F and Supplementary Figure S5J). We independently con-

firmed the methylation status of some target sites using MazF-qPCR assays, that allows interrogating methylation levels at a subset of sites with m^{6}ACA sequence (60). This corroborated Ime4-dependent methylation at the Pho92-binding sites on the *REC8* (at position A + 1461, relative to A of ATG in genomic DNA) and *SAE3* (at position A + 376) transcripts at 3 and 7 h after transfer in SPO medium (Figure 5G). These data indicate that Pho92 is directly binding mRNAs during meiotic prophase and that, most if not all of its targets, in particular those encoding meiotic recombination factors, are m^{6}A-modified at the binding sites.

Pho92 contributes to the down-regulation of its targets

To establish the molecular consequences of RNA binding by Pho92, we examined profiles of meiotic expression determined by RNA-seq for Ime4-dependent Pho92 targets. We only considered hereafter the set of 'high-score' targets to strengthen our conclusions. We first observed that the 208 Pho92 mRNA targets have a higher average expression compared to all genes expressed at 5 h in SPO, the time at which CRAC data were obtained (Figure 6A). Indeed, 148 targets (71%) are among the top 25% of genes with higher expression values at 5 h in SPO in all strains, indicating that Pho92 affects a significant proportion of the transcriptome.

Our analysis of m^{6}A levels and transcriptomic data during meiosis suggest a role for Pho92 in down-regulation of methylated mRNAs at a specific stage of meiosis. Accordingly, the Pho92 mRNA targets accumulate to higher levels at 6, 7 and 9 h in SPO in *pho92Δ/Δ* compared to the WT (Figure 6B and Supplementary Figure S6A). At 6 h in SPO for example, 47 of the 208 Pho92 targets are significantly up-regulated in *pho92Δ/Δ* compared to the WT (Supplementary Figure S6B). A similar effect is seen in the *ime4Δ/Δ* mutant but with a larger variation in expression values and an increased differential expression compared to the WT (Figure 6B and Supplementary Figure S6A-B). Yet, closer inspection of expression profiles of the Pho92 targets during the meiotic time course revealed some temporal heterogeneity. In line with a delayed down-regulation, some targets, reaching their maximum mRNA level at 5 h in SPO in the WT, accumulates to a higher level at 6 h in absence of Pho92 (Supplementary Figure S6C). However, other targets with peaks of expression at 6 and 7 h in SPO in the WT, show a delayed up-regulation in *pho92Δ/Δ* cells (Supplementary Figure S6C). The delayed up-regulation of this second group in absence of Pho92 (or Ime4) is likely an indirect consequence of the dysregulation of earlier phases of meiosis, although we cannot exclude that Pho92 has opposite effects on the temporal expression of different groups of targets. Interestingly, almost all of the 16 targets with functions in meiotic recombination show a similar profile with an extended expression in *pho92Δ/Δ* and *ime4Δ/Δ* compared to WT (Figure 6C). We conclude that Pho92 is specifically required for the down-regulation of its mRNA targets reaching their maximum expression during meiotic prophase that include, in particular, genes associated with meiotic recombination.

Altering m^{6}A sites prevents normal down-regulation of Pho92 targets and slows down meiosis

To investigate whether m^{6}A controls the fate of Pho92 meiotic mRNA targets, we mutated the Pho92-binding sites in the Rec8 and Sae3 mRNAs, 2 transcripts which we confirmed to be methylated by two independent strategies (Figure 5F, G). The mutation A + 1461 > G was introduced in *REC8* while both C + 359 > T and A + 376 > C substitutions were introduced in two close sites in *SAE3*. In both cases, point mutation(s) altered the consensus methylation sequences without changing the encoded protein. The impact of these mutations on accumulation of the corresponding mRNA during meiosis was then assessed by RT-qPCR. In both cases, absence of Pho92 or mutation of the Pho92-binding sites does not alter the amount of *REC8* and *SAE3* mRNAs at 3 and 5 h in SPO (Figure 6D). However, at 6 h, the presence of point mutations abolishes the reduction of *REC8* and *SAE3* mRNA levels observed in WT cells, similarly to the defect observed in the *pho92Δ/Δ* mutant (Figure 6D). This observation prompted us to assay the kinetics of meiosis in these mutant strains. While mutation of the Pho92-binding sites in *SAE3* did not induce a change in the temporal appearance of meiotic cells compared to WT, the point mutant of *REC8* induced a meiotic delayed phenotype similar to the one observed in *pho92Δ/Δ* cells (Figure 6E). Hence, impairing the binding of Pho92 to *REC8* and *SAE3* mRNAs is sufficient to delay their down-regulation, and in the case of *REC8,* it also suffices to delay meiotic divisions, similar to the effects observed in the absence of Pho92. These results establish *REC8* as a critical target of m^{6}A and Pho92 during meiosis.

DISCUSSION

Modification of mRNAs through m^{6}A-methylation has an evolutionarily conserved impact in gametogenesis of many organisms (13,70–72) but the contribution of m^{6}A readers as well as the relevance of individual m^{6}A sites in mRNAs remain poorly known, particularly during yeast meiosis. Here, we provide evidence that Pho92 controls the duration of the meiotic recombination and contributes to the regulation of transcript abundance, particularly of mRNAs encoding meiotic recombination factors. Direct analysis of sites bound by Pho92 reveals functional sites contributing to the meiotic progression in yeast, among which *REC8* appears as a critical target.

We show that Pho92 is an early meiotic factor under the control of a URS1 element in its promoter, allowing both meiotic activation and repression in non-meiotic conditions. Interestingly, the *PHO92* promoter also contains a conserved binding-site for the general transcription activator Abf1 in *Saccharomyces* yeast. The association of an Abf1-binding site and a URS1 element is also found in promoters of *HOP1, RED1* and *ZIP1* (73), 3 actors with specific functions in meiotic recombination. Hence, these data support a specialized function of Pho92 during early meiotic steps. Consistently, we observed that deletion of *PHO92* delays meiosis with a concomitant dysregulation of the meiotic transcriptome profile. Surprisingly, the ab-

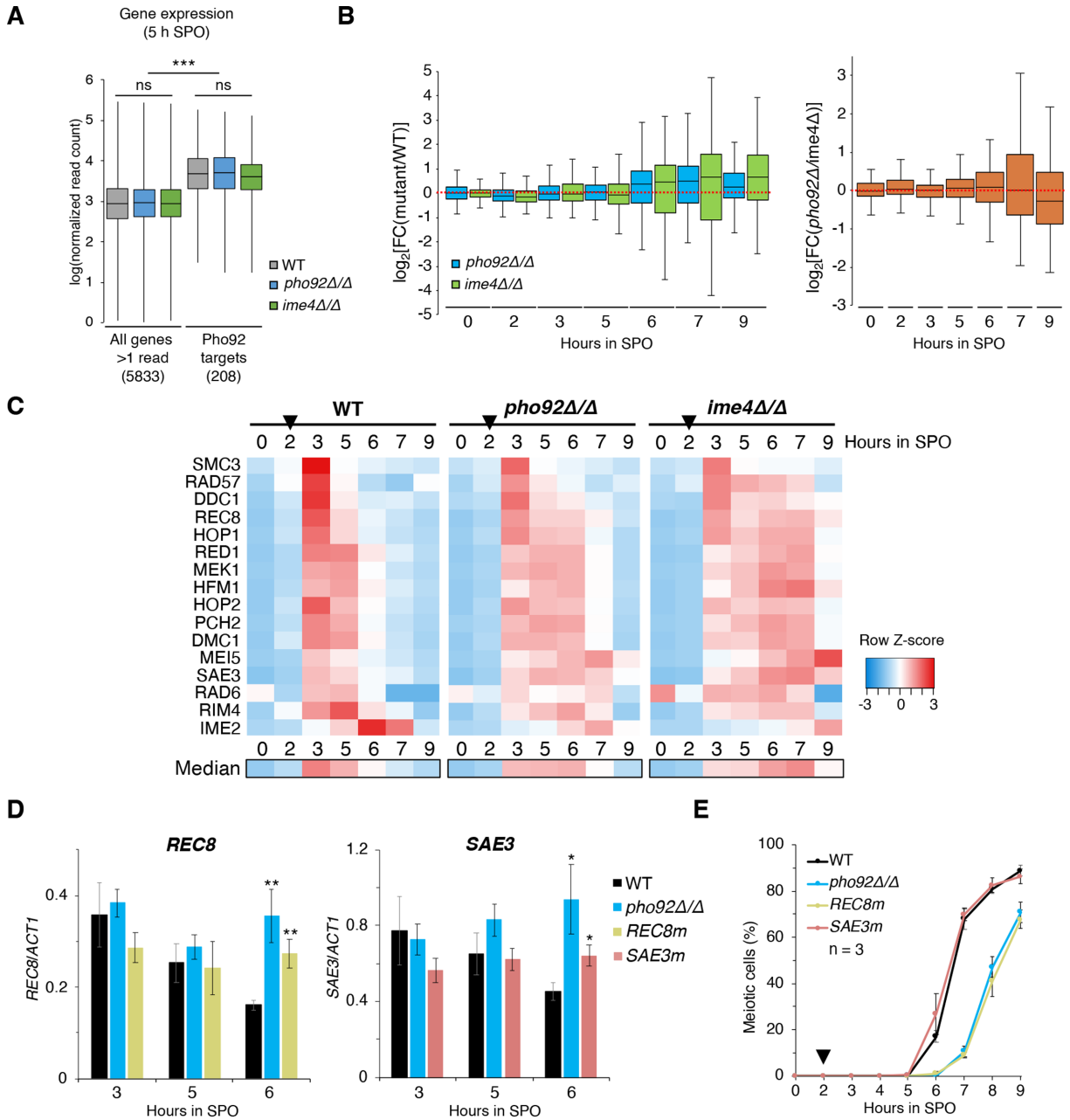

Figure 6. Pho92 contributes to the down-regulation of its meiotic targets including *REC8* and *SAE3*. (**A**) Expression of the Pho92-targets compared to all genes expressed (read > 1) at 5 h in SPO in WT, *pho92Δ/Δ* and *ime4Δ/Δ* cells. The distribution of the $\log_{10}$ normalized read counts of all genes is indicated with box plots (min, first quartile, median, third quartile, max) according to the mean values from three biological replicates. ns: $P > 0.05$, ***$P < 0.001$, two-tailed *t*-test. (**B**) Differential analysis of expression of Pho92 targets in *pho92Δ/Δ* and *ime4Δ/Δ* mutants compared to WT in mRNA-seq data. Left panel: $\log_2$ fold change value of the mean normalized read count of 3 biological replicates of each Pho92 target in *pho92Δ/Δ* mutant (blue) or *ime4Δ/Δ* mutant (green) over the WT across the meiotic time course. Right panel: expression values of the Pho92 targets in the *pho92Δ/Δ* mutant compared to the *ime4Δ/Δ* mutant. (**C**) Heat map representation of expression of 16 Pho92 targets with meiotic functions during the meiotic time course in WT cells, *pho92Δ/Δ* and *ime4Δ/Δ* mutants. *Z*-score transformation was performed for each gene considering the mean normalized read count of three biological replicates and scaled from maximum (red) to minimum (blue) expression value from all samples. A median expression profile from the 16 genes is represented below. Black triangle at 2 h: time of *IME1* induction. (**D**) RT-qPCR analysis of *REC8* (left) and *SAE3* (right) transcripts at 3, 5 and 6 h after SPO resuspension in WT, *pho92Δ/Δ* and respective point mutation strains. *REC8m:* mutation of A + 1461 > G in *REC8*; *SAE3m:* mutations of C + 359 > T and A + 376 > C in *SAE3*. Means and standard deviations from three biological replicates. *$P < 0.05$, **$P < 0.01$, two-tailed *t*-test compared to the WT at each time point. (**E**) Kinetics of meiotic divisions from WT, *pho92Δ/Δ* mutant, *REC8m* and *SAE3m* point mutants used in (D). Meiotic cells correspond to cells containing >1 nucleus as monitored by DAPI staining on 200 cells per time point. Means and standard deviations from three biological replicates. Black triangle above 2 h: time of *IME1* induction.

sence of Pho92 does not phenocopy the deletion of *IME4*, the latter resulting in a more severe lag, both for meiosis progression and for their impact on the transcriptome. It is possible that Ime4 has a function independent of its methylase activity, as suggested by the less severe phenotype induced by the catalytic site mutant of Ime4 (13). Alternatively, other reader protein(s) may be present during yeast meiosis or m^{6}A may act by preventing the binding of some RNA-binding proteins or by altering RNA structures. Further analyses will be required to pinpoint the mechanisms implicated.

Our analysis of transcriptome dynamics reveals that the early stages of meiosis before the onset of meiotic prophase I are unaffected in the absence of m^{6}A or of the m^{6}A reader Pho92 but the absence of one or the other impairs timely meiotic recombination and delays downstream events. Strikingly, meiotic defects start to arise concomitantly to the m^{6}A peaks in WT cells and in absence of Pho92 and Ime4, the first group of genes with extended expression encode factors involved in meiotic recombination. Consistently, DNA replication is not affected but DSBs formation, corresponding to the initiation of meiotic recombination, occurs later in the two mutant strains, with little difference between them. Yet, except for these delays, the same waves of transcripts are up- and down-regulated in WT and the two mutants, suggesting that a key checkpoint must be overcome to allow cells to progress further in meiosis and arguing against a global dysregulation of gene expression.

Large sets of m^{6}A sites had been previously reported in yeast mRNAs during meiosis (14,21,60,74,75). Established using different methods, those show limited overlap, partly owing to distinct experimental parameters (different strains or analyses at different time points) but also possibly due to methodological limitations (76). Despite this large number of m^{6}A sites, the evidence of functional sites able to affect gene expression at molecular levels and/or contributing to physiological functions remain elusive. Until now, only the m^{6}A site of the *RME1* transcript was reported to have an effect leading to its destabilization and indirect *IME1* activation (21). It is important to note, however, that *RME1* is repressed in diploid cells (77) and that the negative effect of Ime4 on its expression was observed several hours after entry in sporulation after the initial Ime1 expression (21), suggesting that the proposed regulation would at best affect late stage of the yeast meiotic program. Our data further question this model as m^{6}A levels resulting from *IME4* induction increase concomitantly with Ime1 accumulation, precluding an effect of m^{6}A on initial Ime1 induction. Further, the meiotic delay resulting from Pho92 inactivation is detected even after *IME1* induction in the *pCUP-IME1* background which bypasses Rme1 control. Altogether, the contribution of m^{6}A and *RME1* to the initial induction of *IME1* during meiosis, if any, remains to be clarified.

To identify functional sites bound by Pho92 in an Ime4-dependent manner during yeast meiosis, we performed a CRAC analysis, a strategy that bypasses possible biases associated with immuno-enrichment of m^{6}A residues. The CRAC data appeared robust, with a good signal to noise ratio and with most Pho92 mRNA targets being clearly Ime4-dependent. At least in the cases of *SAE3* and *REC8* transcripts, the presence of methylated residues at different meiotic time points could be confirmed by independent MazF-qPCR assays. If one could have envisaged that Pho92 binds non-methylated mRNAs, our CRAC data argue against this. Indeed, in the absence of Ime4, Pho92 fails to bind to its target mRNAs even though those are expressed, and 'Ime4-independent' Pho92 binding sites appear to be nearly exclusively in non-coding RNAs. Yet, our Pho92 CRAC analysis identified significantly less modified mRNAs compared to previous analyses. Only 18–45% of Pho92-binding sites revealed by our study were also reported as methylated in 2 methodologically independent studies (14,60) (Supplementary Figure S5J). While some biological parameters (e.g. time point during meiosis or strain) may contribute to these differences, they could also be explained if the Pho92 reader only binds a subset of the methylated A residues, a possibility that will require further investigation.

It is noteworthy that the absence of Pho92 results in a prolonged presence of m^{6}A and delayed down-regulation of transcripts belonging to the earliest affected clusters. Consistent with previous studies linking m^{6}A readers with mRNA decay (25,28), we propose that Pho92 facilitates prophase exit by favoring the down-regulation of key transcripts, notably those involved in meiotic recombination (Figure 7). Yet, the functional link between Pho92 and the decay machinery remains to be clarified. Identified Ime4-dependent targets of Pho92 include *REC8*, *HOP1* and *RED1*, encoding the core components of axial elements of the synaptonemal complexes that link homologous pairs of sister chromatids during meiotic recombination (78). Rec8 is a meiosis specific member of the cohesin complex with major functions in cohesion of sister chromatids, formation of chromosome axis and promotion of reciprocal recombination during meiosis (79,80). Alteration of either expression or clearance of Rec8 protein levels during meiosis impairs the beginning of the meiotic divisions (79,81). Other meiotic targets of Pho92 comprise the transcript of Mek1, whose activity is linked to DSBs formation and is required for the meiotic recombination checkpoint (67,82), and of Sae3 who is needed for full assembly of the synaptonemal complexes and DSBs reparation (83). Given that alteration of *SAE3* and *MEK1* expression impairs the meiotic prophase arrest, this further support that Pho92 controls transcript abundance of key actors in the establishment of meiotic checkpoints. Interestingly, we also observed, by MazF-qPCR assays, that *REC8* and *SAE3* mRNAs are methylated at 3 hr in SPO when no difference in the steady state levels of theses transcripts was observed between WT and *pho92Δ/Δ* mutant. This suggests that the m^{6}A effect on transcript degradation through Pho92 is temporally regulated. One hypothesis that we did not explore is whether Pho92 could promote translation of its targets before facilitating their down-regulation, in agreement with the presence of m^{6}A in translating ribosomes (84) and described functions of YTHDFs readers in mammals (26).

The identification of m^{6}A sites bound by the Pho92 reader protein raised the question of whether those were functional. To test this possibility, we mutated sites present in the *SAE3* and *REC8* mRNAs (without altering their coding capacity). Interestingly, these subtle changes were sufficient to impair the down-regulation of these transcripts at late meiotic prophase, similarly to those observed in the ab-

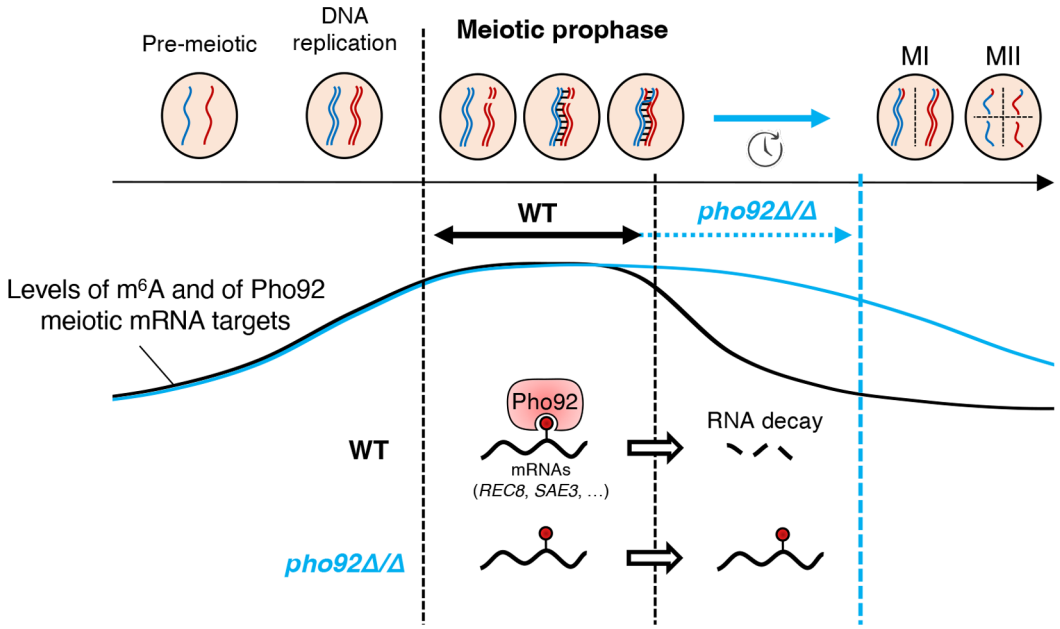

Figure 7. A model for the function of the m^{6}A reader Pho92 in the yeast meiotic program. Pho92 promotes the down-regulation of key methylated targets (*REC8* or *SAE3* for example) at late meiotic prophase. The subsequent down-regulation of these mRNAs targets, occurring once they reach their maximum of expression at the onset of meiotic recombination, allows the cells to progress into the downstream events of meiotic divisions. In absence of Pho92, these methylated targets persist and the prophase exit is delayed. A similar persistence of individual mRNA(s) occurs when functional m^{6}A site(s) that they carry has (have) been mutated to prevent Ime4-dependent methylation.

sence of Pho92. In the case of *REC8*, the point mutant also delayed the kinetics of meiosis. The latter is consistent with the Rec8 factor being one key actor in temporal control of prophase exit, thus its extended expression potentially impairs the disassembly of the synaptonemal complexes and prolongs prophase I. In contrast, mutations of the m^{6}A site in the *SAE3* mRNA had no detectable consequences on meiosis kinetics. This suggests that the global effect of the absence of Pho92 on meiosis will be the cumulative result of the absence of m^{6}A in all of its targets, some possibly speeding the meiotic progression, others having no effect and some delaying it. Thus, our data provide new insights in the complex role of an m^{6}A reader in a highly dynamic differentiation program in yeast.

DATA AVAILABILITY

RNA-seq and CRAC data have been deposited in the Gene Expression Omnibus (GEO) under accession GSE200089. All data is available from the authors upon reasonable request.

NOTE ADDED IN PROOF

Independent work on Pho92 has been recently uploaded on bioRxiv: Varier et al. m6A reader Pho92 is recruited co-transcriptionally and couples translation efficacy to mRNA decay to promote meiotic fitness in yeast. bioRxiv 2022.01.20.477035; doi: https://doi.org/10.1101/2022.01.20.477035.

SUPPLEMENTARY DATA

Supplementary Data are available at NAR Online.

ACKNOWLEDGEMENTS

We acknowledge our team members for support and suggestions. We also thank N. Hollingsworth for the kind gift of antibodies, F. van Werven for kindly sharing the *pCUP-IME1* strain, A. Nicolas for the SK1 strain, IGBMC platforms particularly the GenomEast, Imaging, Mediaprep and FACS facilities for support, the I2BC sequencing platform, and D. Heintz and C. Villette for help with m^{6}A quantification.

Author contributions: Experimental design, J.S. and B.S.; experiments realization J.S., D.P., M.M. T.V., J.Z.; writing of original draft, J.S. and B.S.; manuscript reviewing, J.S., D.P., T.V., J.Z., D.L., B.S.; funding, D.L. and B.S.; project supervision, D.L. and B.S.

FUNDING

Ligue Contre le Cancer (Equipe Labellisée 2020) [to B.S.]; Agence Nationale pour la Recherche [ANR-16-CE11-0003 to B.S.]; CERBM-IGBMC [to B.S.]; Interdisciplinary Thematic Institute IMCBio, as part of the ITI 2021–2028 program of the University of Strasbourg, CNRS and Inserm, was supported by IdEx Unistra [ANR-10-IDEX-0002]; SFRI-STRAT'US project [ANR 20-SFRI-0012]; EUR IMCBio [ANR-17-EURE-0023] under the framework of the French Investments for the Future Program. The GenomEast platform is a member of the 'France

Génomique' consortium [ANR-10-INBS-0009]. Funding for open access charge: Ligue contre le Cancer.
Conflict of interest statement. None declared.

REFERENCES

1. Klungland,A., Dahl,J.A., Greggains,G., Fedorcsak,P. and Filipczyk,A. (2017) Reversible RNA modifications in meiosis and pluripotency. *Nat. Methods*, **14**, 18–22.
2. Hsu,P.J., Shi,H. and He,C. (2017) Epitranscriptomic influences on development and disease. *Genome Biol.*, **18**, 197.
3. Du,K., Zhang,L., Lee,T. and Sun,T. (2019) m6A RNA methylation controls neural development and is involved in human diseases. *Mol. Neurobiol.*, **56**, 1596–1606.
4. Chen,X.Y., Zhang,J. and Zhu,J.S. (2019) The role of m6A RNA methylation in human cancer. *Mol. Cancer*, **18**, 103.
5. Mauer,J., Luo,X., Blanjoie,A., Jiao,X., Grozhik,A.v., Patil,D.P., Linder,B., Pickering,B.F., Vasseur,J.-J., Chen,Q. *et al.* (2017) Reversible methylation of m6Am in the 5′ cap controls mRNA stability. *Nature*, **541**, 371–375.
6. Zaccara,S., Ries,R.J. and Jaffrey,S.R. (2019) Reading, writing and erasing mRNA methylation. *Nat. Rev. Mol. Cell Biol.*, **20**, 608–624.
7. Zhong,S., Li,H., Bodi,Z., Button,J., Vespa,L., Herzog,M. and Fray,R.G. (2008) MTA is an arabidopsis messenger RNA adenosine methylase and interacts with a homolog of a sex-specific splicing factor. *Plant Cell*, **20**, 1278–1288.
8. Slobodin,B., Han,R., Calderone,V., Vrielink,J.A.F.O., Loayza-Puch,F., Elkon,R. and Agami,R. (2017) Transcription impacts the efficiency of mRNA translation via Co-transcriptional N6-adenosine methylation. *Cell*, **169**, 326–337.
9. Śledź,P. and Jinek,M. (2016) Structural insights into the molecular mechanism of the m6A writer complex. *Elife*, **5**, e18434.
10. Wang,P., Doxtader,K.A. and Nam,Y. (2016) Structural basis for cooperative function of mettl3 and mettl14 methyltransferases. *Mol. Cell*, **63**, 306–317.
11. Wang,X., Feng,J., Xue,Y., Guan,Z., Zhang,D., Liu,Z., Gong,Z., Wang,Q., Huang,J., Tang,C. *et al.* (2016) Structural basis of N6-adenosine methylation by the METTL3–METTL14 complex. *Nature*, **534**, 575–578.
12. Clancy,M.J., Shambaugh,M.E., Timpte,C.S. and Bokar,J.A. (2002) Induction of sporulation in saccharomyces cerevisiae leads to the formation of N6-methyladenosine in mRNA: a potential mechanism for the activity of the IME4 gene. *Nucleic Acids Res.*, **30**, 4509–4518.
13. Agarwala,S.D., Blitzblau,H.G., Hochwagen,A. and Fink,G.R. (2012) RNA methylation by the MIS complex regulates a cell fate decision in yeast. *PLoS Genet.*, **8**, e1002732.
14. Schwartz,S., Agarwala,S.D., Mumbach,M.R., Jovanovic,M., Mertins,P., Shishkin,A., Tabach,Y., Mikkelsen,T.S., Satija,R., Ruvkun,G. *et al.* (2013) High-Resolution mapping reveals a conserved, widespread, dynamic mRNA methylation program in yeast meiosis. *Cell*, **155**, 1409–1421.
15. Piekarska,I., Rytka,J. and Rempola,B. (2010) Regulation of sporulation in the yeast saccharomyces cerevisiae. *Acta Biochim. Pol.*, **57**, 241–250.
16. Neiman,A.M. (2011) Sporulation in the budding yeast saccharomyces cerevisiae. *Genetics*, **189**, 737–765.
17. Jin,L. and Neiman,A.M. (2016) Post-transcriptional regulation in budding yeast meiosis. *Curr. Genet.*, **62**, 313–315.
18. Eisenberg,A.R., Higdon,A., Keskin,A., Hodapp,S., Jovanovic,M. and Brar,G.A. (2018) Precise Post-translational tuning occurs for most protein complex components during meiosis. *Cell Rep.*, **25**, 3603–3617.
19. Hongay,C.F., Grisafi,P.L., Galitski,T. and Fink,G.R. (2006) Antisense transcription controls cell fate in saccharomyces cerevisiae. *Cell*, **127**, 735–745.
20. van Werven,F.J., Neuert,G., Hendrick,N., Lardenois,A., Buratowski,S., van Oudenaarden,A., Primig,M. and Amon,A. (2012) Transcription of two long noncoding RNAs mediates mating-type control of gametogenesis in budding yeast. *Cell*, **150**, 1170–1181.
21. Bushkin,G.G., Pincus,D., Morgan,J.T., Richardson,K., Lewis,C., Chan,S.H., Bartel,D.P. and Fink,G.R. (2019) m6A modification of a 3′ UTR site reduces RME1 mRNA levels to promote meiosis. *Nat. Commun.*, **10**, 3414 .
22. Xiao,W., Adhikari,S., Dahal,U., Chen,Y., Hao,Y., Sun,B. and Sun,H. (2016) Nuclear m6A reader YTHDC1 regulates mRNA splicing. *Mol. Cell*, **61**, 507–519.
23. Roundtree,I.A., Luo,G.-Z., Zhang,Z., Wang,X., Zhou,T., Cui,Y., Sha,J., Huang,X., Guerrero,L., Xie,P. *et al.* (2017) YTHDC1 mediates nuclear export of N6-methyladenosine methylated mRNAs. *Elife*, **6**, e31311.
24. Wang,X., Lu,Z., Gomez,A., Hon,G.C., Yue,Y., Han,D., Fu,Y., Parisien,M., Dai,Q., Jia,G. *et al.* (2014) N6-methyladenosine-dependent regulation of messenger RNA stability. *Nature*, **505**, 117–120.
25. Du,H., Zhao,Y., He,J., Zhang,Y., Xi,H., Liu,M., Ma,J. and Wu,L. (2016) YTHDF2 destabilizes m6A-containing RNA through direct recruitment of the CCR4–NOT deadenylase complex. *Nat. Commun.*, **7**, 12626.
26. Wang,X., Zhao,B.S., Roundtree,I.a., Lu,Z., Han,D., Ma,H., Weng,X., Chen,K., Shi,H. and He,C. (2015) N6-methyladenosine modulates messenger RNA translation efficiency. *Cell*, **161**, 1388–1399.
27. Shi,H., Wang,X., Lu,Z., Zhao,B.S., Ma,H., Hsu,P.J. and He,C. (2017) YTHDF3 facilitates translation and decay of N6-methyladenosine-modified RNA. *Cell Res.*, **27**, 315–328.
28. Zaccara,S. and Jaffrey,S.R. (2020) A unified model for the function of YTHDF proteins in regulating m6A-Modified mRNA. *Cell*, **181**, 1582–1595.
29. Lasman,L., Krupalnik,V., Viukov,S., Mor,N., Aguilera-Castrejon,A., Schneir,D., Bayerl,J., Mizrahi,O., Peles,S., Tawil,S. *et al.* (2020) Context-dependent compensation between functional ythdf m6A reader proteins. *Genes Dev.*, **34**, 1373–1391.
30. Kontur,C., Jeong,M., Cifuentes,D. and Giraldez,A.J. (2020) Ythdf m6A readers function redundantly during zebrafish development. *Cell Rep.*, **33**, 108598.
31. Kang,H.-J., Jeong,S.-J., Kim,K.-N., Baek,I.-J., Chang,M., Kang,C.-M., Park,Y.-S. and Yun,C.-W. (2014) A novel protein, pho92, has a conserved YTH domain and regulates phosphate metabolism by decreasing the mRNA stability of PHO4 in saccharomyces cerevisiae. *Biochem. J.*, **457**, 391–400.
32. Scutenaire,J., Deragon,J.M., Jean,V., Benhamed,M., Raynaud,C., Favory,J.J., Merret,R. and Bousquet-Antonelli,C. (2018) The YTH domain protein ECT2 is an m6A reader required for normal trichome branching in arabidopsis. *Plant Cell*, **30**, 986–1005.
33. Xu,C., Liu,K., Ahmed,H., Loppnau,P., Schapira,M. and Min,J. (2015) Structural basis for the discriminative recognition of n 6-Methyladenosine RNA by the human YT521-B homology domain family of proteins. *J. Biol. Chem.*, **290**, 24902–24913.
34. Chia,M. and van Werven,F.J. (2016) Temporal expression of a master regulator drives synchronous sporulation in budding yeast. *G3: Genes Genomes Genetics*, **6**, 3553–3560.
35. Guthrie,C. and Fink,G. (2002) In: *Guide to Yeast Genetics and Molecular and Cell Biology - Parts B*. Elsevier.
36. Granneman,S., Kudla,G., Petfalski,E. and Tollervey,D. (2009) Identification of protein binding sites on U3 snoRNA and pre-rRNA by UV cross-linking and high-throughput analysis of cDNAs. *Proc. Natl. Acad. Sci. U.S.A.*, **106**, 9613–9618.
37. Kushnirov,V.v. (2000) Rapid and reliable protein extraction from yeast. *Yeast*, **16**, 857–860.
38. Zhang,T., Lei,J., Yang,H., Xu,K., Wang,R. and Zhang,Z. (2011) An improved method for whole protein extraction from yeast saccharomyces cerevisiae. *Yeast*, **28**, 795–798.
39. de los Santos,T. and Hollingsworth,N.M. (1999) Red1p, a MEK1-dependent phosphoprotein that physically interacts with hop1p during meiosis in yeast. *J. Biol. Chem.*, **274**, 1783–1790.
40. Busygina,V., Sehorn,M.G., Shi,I.Y., Tsubouchi,H., Roeder,G.S. and Sung,P. (2008) Hed1 regulates Rad51-mediated recombination via a novel mechanism. *Genes Dev.*, **22**, 786–795.
41. Callender,T.L., Laureau,R., Wan,L., Chen,X., Sandhu,R., Laljee,S., Zhou,S., Suhandynata,R.T., Prugar,E., Gaines,W.A. *et al.* (2016) Mek1 down regulates rad51 activity during yeast meiosis by phosphorylation of hed1. *PLoS Genet.*, **12**, e1006226.
42. Altschup,S.F., Gish,W., Miller,W., Myers,E.W. and Lipman,D.J. (1990) Basic local alignment search tool. *J. Mol. Biol.*, **215**, 403–410.
43. Thompson,J.D., Gibson,T.J., Plewniak,F., Jeanmougin,F. and Higgins,D.G. (1997) The CLUSTAL_X windows interface: flexible

strategies for multiple sequence alignment aided by quality analysis tools. *Nucleic Acids Res.*, **25**, 4876–4882.
44. Waterhouse,A.M., Procter,J.B., Martin,D.M.A., Clamp,M. and Barton,G.J. (2009) Jalview version 2-A multiple sequence alignment editor and analysis workbench. *Bioinformatics*, **25**, 1189–1191.
45. Kim,D., Pertea,G., Trapnell,C., Pimentel,H., Kelley,R. and Salzberg,S.L. (2013) TopHat2: accurate alignment of transcriptomes in the presence of insertions, deletions and gene fusions. *Genome Biol.*, **14**, R36.
46. Langmead,B., Trapnell,C., Pop,M. and Salzberg,S.L. (2009) Ultrafast and memory-efficient alignment of short DNA sequences to the human genome. *Genome Biol.*, **10**, R25.
47. Anders,S., Pyl,P.T. and Huber,W. (2015) HTSeq-A python framework to work with high-throughput sequencing data. *Bioinformatics*, **31**, 166–169.
48. Love,M.I., Huber,W. and Anders,S. (2014) Moderated estimation of fold change and dispersion for RNA-seq data with DESeq2. *Genome Biol.*, **15**, 550.
49. Anders,S. and Huber,W. (2010) Differential expression analysis for sequence count data. *Genome Biol.*, **11**, R106.
50. Benjamini,Y. and Hochberg,Y. (1995) Controlling the false discovery rate: a practical and powerful approach to multiple testing. *J. Roy. Statist. Soc. Ser. C*, **57**, 289–300.
51. Kumar,L. and Futschik,M. (2007) Software mfuzz: a software package for soft clustering of microarray data. *Bioinformation*, **2**, 5–7.
52. Babicki,S., Arndt,D., Marcu,A., Liang,Y., Grant,J.R., Maciejewski,A. and Wishart,D.S. (2016) Heatmapper: web-enabled heat mapping for all. *Nucleic Acids Res.*, **44**, W147–W153.
53. Murakami,H., Borde,V., Nicolas,A. and Keeney,S. (2009) Gel electrophoresis assays for analyzing DNA double-strand breaks in saccharomyces cerevisiae at various spatial resolutions. *Methods Mol. Biol.*, **557**, 117–142.
54. Rai,S.K., Atwood-Moore,A. and Levin,H.L. (2018) High-frequency lithium acetate transformation of schizosaccharomyces pombe. *Methods Mol. Biol.*, **1721**, 167–177.
55. Matsuo,Y., Asakawa,K., Toda,T. and Katayama,S. (2006) A rapid method for protein extraction from fission yeast. *Biosci. Biotechnol. Biochem.*, **70**, 1992–1994.
56. Villa,T., Barucco,M., Martin-Niclos,M.J., Jacquier,A. and Libri,D. (2020) Degradation of Non-coding RNAs promotes recycling of termination factors at sites of transcription. *Cell Rep.*, **32**, 107942.
57. Candelli,T., Gros,J. and Libri,D. (2018) Pervasive transcription fine-tunes replication origin activity. *Elife*, **7**, e40802.
58. Bailey,T.L., Johnson,J., Grant,C.E. and Noble,W.S. (2015) The MEME suite. *Nucleic Acids Res.*, **43**, W39–W49.
59. Xijin Ge,S., Jung,D. and Yao,R. (2020) ShinyGO: a graphical gene-set enrichment tool for animals and plants. *Bioinformatics*, **36**, 2628–2629.
60. Garcia-Campos,M.A., Edelheit,S., Toth,U., Safra,M., Shachar,R., Viukov,S., Winkler,R., Nir,R., Lasman,L., Brandis,A. *et al.* (2019) Deciphering the "m6A code" via antibody-independent quantitative profiling. *Cell*, **178**, 731–747.
61. Primig,M., Williams,R.M., Winzeler,E.A., Tevzadze,G.G., Conway,A.R., Hwang,S.Y., Davis,R.W. and Esposito,R.E. (2000) The core meiotic transcriptome in budding yeasts. *Nat. Genet.*, **26**, 415–423.
62. Chu,S. and Herskowitz,I. (1998) Gametogenesis in yeast is regulated by a transcriptional cascade dependent on ndt80. *Mol. Cell*, **1**, 685–696.
63. Rossi,M.J., Kuntala,P.K., Lai,W.K.M., Yamada,N., Badjatia,N., Mittal,C., Kuzu,G., Bocklund,K., Farrell,N.P., Blanda,T.R. *et al.* (2021) A high-resolution protein architecture of the budding yeast genome. *Nature*, **592**, 309–314.
64. Deutschbauer,A.M., Williams,R.M., Chu,A.M. and Davis,R.W. (2002) Parallel phenotypic analysis of sporulation and postgermination growth in saccharomyces cerevisiae. *Proc. Natl. Acad. Sci. U.S.A.*, **99**, 15530–15535.
65. Niu,H., Wan,L., Baumgartner,B., Schaefer,D., Loidl,J. and Hollingsworth,N.M. (2005) Partner choice during meiosis is regulated by Hop1-promoted dimerization of mek1. *Mol. Biol. Cell*, **16**, 5804–5818.
66. Carballo,J.A., Johnson,A.L., Sedgwick,S.G. and Cha,R.S. (2008) Phosphorylation of the axial element protein hop1 by mec1/tel1 ensures meiotic interhomolog recombination. *Cell*, **132**, 758–770.
67. Prugar,E., Burnett,C., Chen,X. and Hollingsworth,N.M. (2017) Coordination of double strand break repair and meiotic progression in yeast by a mek1-ndt80 negative feedback loop. *Genetics*, **206**, 497–512.
68. Baudat,F. and Nicolas,A. (1997) Clustering of meiotic double-strand breaks on yeast chromosome III. *Proc. Natl. Acad. Sci. U.S.A.*, **94**, 5213–5218.
69. Buhler,C., Borde,V. and Lichten,M. (2007) Mapping meiotic single-strand DNA reveals a new landscape of DNA double-strand breaks in saccharomyces cerevisiae. *PLoS Biol.*, **5**, 2797–2808.
70. Hsu,P.J., Zhu,Y., Ma,H., Guo,Y., Shi,X., Liu,Y., Qi,M., Lu,Z., Shi,H., Wang,J. *et al.* (2017) Ythdc2 is an N6-methyladenosine binding protein that regulates mammalian spermatogenesis. *Cell Res.*, **27**, 1115–1127.
71. Wojtas,M.N., Pandey,R.R., Mendel,M., Homolka,D., Sachidanandam,R. and Pillai,R.S. (2017) Regulation of m6A transcripts by the 3′→5′ RNA helicase YTHDC2 is essential for a successful meiotic program in the mammalian germline. *Mol. Cell*, **68**, 374–387.
72. Xu,K., Yang,Y., Feng,G., Sun,B., Chen,J., Li,Y. and Chen,Y. (2017) Mettl3-mediated m 6 a regulates spermatogonial differentiation and meiosis initiation. *Cell Res.*, **27**, 1100–1114.
73. Gailus-Durner,V., Xie,J., Chintamaneni,C. and Vershon,A.K. (1996) Participation of the yeast activator abf1 in meiosis-specific expression of the HOP1 gene. *Mol. Cell. Biol.*, **16**, 2777–2786.
74. Dierks,D., Garcia-Campos,M.A., Uzonyi,A., Safra,M., Edelheit,S., Rossi,A., Sideri,T., Varier,R.A., Brandis,A., Stelzer,Y. *et al.* (2021) Multiplexed profiling facilitates robust m6A quantification at site, gene and sample resolution. *Nat. Methods*, **18**, 1060–1067.
75. Leger,A., Amaral,P.P., Pandolfini,L., Capitanchik,C., Capraro,F., Miano,V., Migliori,V., Toolan-Kerr,P., Sideri,T., Enright,A.J. *et al.* (2021) RNA modifications detection by comparative nanopore direct RNA sequencing. *Nat. Commun.*, **12**, 7198.
76. McIntyre,A.B.R., Gokhale,N.S., Cerchietti,L., Jaffrey,S.R., Horner,S.M. and Mason,C.E. (2020) Limits in the detection of m6A changes using merip/m6a-seq. *Sci. Rep.*, **10**, 6590.
77. van Werven,F.J. and Amon,A. (2011) Regulation of entry into gametogenesis. *Philos. Trans. Roy. Soc. B: Biol. Sci.*, **366**, 3521–3531.
78. Zickler,D. and Kleckner,N. (2015) Recombination, pairing, and synapsis of homologs during meiosis. *Cold Spring Harb. Perspect. Biol.*, **7**, a016626.
79. Brar,G.A., Hochwagen,A., Ee,L.-S.S. and Amon,A. (2009) The multiple roles of cohesin in meiotic chromosome morphogenesis and pairing. *Mol. Biol. Cell*, **20**, 1030–1047.
80. Yoon,S.W., Lee,M.S., Xaver,M., Zhang,L., Hong,S.G., Kong,Y.J., Cho,H.R., Kleckner,N. and Kim,K.P. (2016) Meiotic prophase roles of rec8 in crossover recombination and chromosome structure. *Nucleic Acids Res.*, **44**, 9296–9314.
81. Brar,G.A., Kiburz,B.M., Zhang,Y., Kim,J.E., White,F. and Amon,A. (2006) Rec8 phosphorylation and recombination promote the step-wise loss of cohesins in meiosis. *Nature*, **441**, 532–536.
82. Wu,H.Y., Ho,H.C. and Burgess,S.M. (2010) Mek1 kinase governs outcomes of meiotic recombination and the checkpoint response. *Curr. Biol.*, **20**, 1707–1716.
83. Hayase,A., Takagi,M., Miyazaki,T., Oshiumi,H., Shinohara,M. and Shinohara,A. (2004) A protein complex containing mei5 and sae3 promotes the assembly of the meiosis-specific RecA homolog dmc1. *Cell*, **119**, 927–940.
84. Bodi,Z., Bottley,A., Archer,N., May,S. and Fray,R.G. (2015) Yeast m6A methylated mRNAs are enriched on translating ribosomes during meiosis, and under rapamycin treatment. *PLoS One*, **10**, e0132090.
85. de Boer,C.G. and Hughes,T.R. (2012) YeTFaSCo: a database of evaluated yeast transcription factor sequence specificities. *Nucleic Acids Res.*, **40**, D169–D179.